

We thank both reviewers again for their constructive comments. Our point-by-point response to their comments is highlighted in bold in this document.

Reviewer #1

5 I enjoyed reading this new version of the manuscript: it is now well-composed and the importance of physical processes and ^{238}U variability on the estimation of downward ^{234}Th export fluxes is clear. I recommend acceptance following minor revisions.

Introduction

10 Line 43. There are many more studies investigating the elemental export fluxes. Please add “e.g.” [Bhat et al., 1968, etc.]

Response: fixed

15 Line 50. and “is” [thus strongly scavenged..]

Response: fixed

Line 55. You can also add Si to the list C, N, P, trace metals.

20

Response: fixed

Line 55. I also would add “e.g.” [Bhat et al., 1968, etc..] as it is a succinct list of studies investigating elemental export fluxes.

25

Response: fixed

Lines 74-75: I think this paragraph break is not necessary. Both paragraphs speak about advection and diffusion effect on ^{234}Th fluxes.

30

Response: We consider the paragraph break appropriate, as the previous paragraph discussed how the single box ^{234}Th models are inappropriate in parts of the open ocean and the second paragraph discussed how ^{234}Th fluxes in coastal regions are more vulnerable to physical processes. This paragraph break is also necessary to avoid a super long paragraph.

35

Line 75. I think you can delete “that” and add “to” [be included..]

Response: For clarity, we modified the sentence as “The dynamic nature of coastal processes requires that physical terms should be included in ^{234}Th flux calculation whenever possible.”

40

Methods

45 Lines 140-147: Please mention why Mn would be a problem during the ICP MS analyses of ^{229}Th / ^{230}Th ratios.

50 **Response: Mn was not a problem for ^{229}Th / ^{230}Th ratios but for the maintenance of ICPMS itself. The large amount of Mn in the samples means that the ICPMS needs to be cleaned thoroughly for days after each ^{229}Th / ^{230}Th session before other trace-metal users could use it again. Performing column chemistry to remove Mn in ^{234}Th samples before ICPMS analysis is now an agreement among lab users in our group.**

55 Line 149: Why do you use 1N HNO₃? Usually ICPMS analyses are made with 2% HNO₃ (i.e. 0.3N).

60 **Response: It is not uncommon to dilute samples in 1N HNO₃ for ICPMS analysis. Typical ICPMS standard solutions are in 2% (0.32N) - 5% (0.8N) HNO₃ solutions, and a few are in 10% (1.6N) HNO₃ solutions. Our lab has been using 1N HNO₃ for ICPMS analyses, which has been working perfectly well for various trace elements.**

65 Lines 164-166: The recommended time interval between two visits is of >2 weeks. What would a time interval of maximum 4.5 days imply for your study?

70 **Response: We modified line 362-364 in Results to address this comment: “The large errors associated with the non-steady state calculation due to the short duration between station occupations prevent a meaningful application of this model in the current study (also see discussion in Resplandy et al, 2012).”**

75 Lines 175-185: I understand the depth for estimating the export fluxes is only of little relevance, but please, indicate at which depths you estimated the fluxes here and why these depths: 100m (for comparing with other studies) and 5-20m below the ML (not exact ML because of sampling logistics).

80 **Response: The reasoning on at which depths fluxes were calculated were originally given in lines 372-376 (Results section): “Due to sampling logistics, we did not sample at the base of the ML, but 5-20 m below the ML. This depth corresponded closely to the EZ depth used in Black et al. (2018) in the same study area during austral spring 2013. For the purpose of comparison with earlier studies which reported ^{234}Th fluxes at 100 m, we also calculated ^{234}Th fluxes at 100 m in this study.” We now moved this paragraph to Line 185.**

85 Lines 205-207: Please give the values of the Coriolis parameter (f) and the water density (ρ) you used and from where they come from.

Response: The Coriolis parameter is not a fixed value but a function of latitude. We now specified the water density in the text.

90 Line 223: Please, precise how you estimate the upwelling rate from the vertical velocity (w)? By interpolation between 0 and 240m?

95 **Response:** The reviewer is correct that upwelling rate was interpolated between 0 and 240 m. We also stated in the original text that “We assumed a linear decrease of w from base of the mixed layer toward both the ocean surface and 240 m depth (bottom depth of our shallowest station). Upwelling rates at any depth between 0 and 240 m at individual stations could thus be determined once w was estimated.”

Lines 236-237: Please mention where these velocities can be found. In Lüdke et al., in review?

100 **Response:** We now referenced (Lüdke et al., in review 2020).

Lines 246-247: Which other cruises are you referencing?

105 **Response:** We now specified M137 as the follow-up cruise.

Line 251: “At most CTD stations”: for which stations do you not have microstructure profiles?

110 **Response:** For clarification, we modified this sentence to state “On transit between each CTD station 3 to 9 microstructure profiles were collected”. Please also note that we stated in Line 261, “An average turbulent vertical diffusivity profile was calculated from all inshore (<500m water depth) and from all offshore (>500m water depth) profiles (Figure S1)”. So we would like to reiterate that inshore and offshore vertical diffusivity profiles are not individual profiles, but averages of all relevant microstructure profiles in proximation to our CTD stations during cruise M136 and M137.

115 Line 255: Which value did you use for the stratification (N) and from where does it come from?

120 **Response:** Stratification (Buoyancy frequency) was calculated using CTD data retrieved from microstructure profilers and following the $gsw_Nsquared$ function from the Gibbs Sea Water library (McDougall et al., 2009; Roquet et al., 2015). A running mean of 10 dbar was applied to avoid including unstable events due to turbulent overturns. We now added this discussion to the text.

125 Line 277: Why do you use $\tau^{1/2}$? Please remove $1/2$ if not needed.

Response: We now use τ_{Th} as 234Th residence time to avoid confusion with τ (wind stress)

Line 284: Please precise the surface layers are until 30m for M136 and 50m for M138, and explain why these depths.

130 **Response:** To avoid repetition throughout the text, we now added in Line 243: “As representative for the near-surface flow, we extracted the velocity data from the top 30 m for M136 stations and top 50 m for M138 station (defined as the “top layer” thereafter); these depths correspond to 5-20 m below the base of the ML during each cruise.” Note that we’ve opted to use the term “top layer” throughout the text instead of “surface layer” to avoid confusion.

135

Results

140 Line 305: Total ²³⁴Th “activities”

Response: fixed

Line 310: Please cite Table 1, where equilibrium depths are showed.

145

Response: fixed

Line 326: Why do you use top layers as top 30m and top 50m? If you agree with one of my previous comment this will be explained in the Methods (line 284).

150

Response: Please refer to our replies in Lines 73 and 128 in this document.

Line 397: Within the *upper* (?) 27 and 33m layer at *offshore* (?) deep stations

155

Response: fixed

Line 415: please provide again the depths of the surface layer.

Response: Please refer to our reply in Line 128 in this document.

160

Lines 420-421: I think this paragraph break is not necessary. Both paragraphs speak about horizontal advection and diffusion effect on ²³⁴Th fluxes.

165 **Response: The former paragraph discussed advection fluxes and the latter one discussed diffusive fluxes. It would be better to have the paragraph break.**

Discussion

Line 443: Delete recent (it was 14 and 9 years ago already!)

170

Response: fixed

Line 446: “a minute increase” is not clear. Do you mean that even a short-term oxygenation event, of the order of the minute, could release U from the sediments? If it is the case, please re write.

175

Response: “a minute increase” means an increase of oxygen of an extremely tiny amount, often below detection limits. We feel that the wording “minute” best described in a scientific manner such extremely small change in oxygen concentrations.

180

Lines 461-479: The explanation is not yet clear. Understanding how U (or Fe) reduction and remobilization could occur “at the same time” was not straightforward at first reading. Please,

make a clear distinction between the ocean-sediment interface where O₂ concentrations can increase, realising U; and the suboxic/anoxic sediments where U is reduced and trapped.

185 Is there a study you could cite to support that a strong El Nino event (such as the one preceding your cruise) could induce an oxygenation event large enough to release U (lines 472-473)?

Response: We agreed with the reviewer and have now added the following discussion to Line 468: “In reducing pore water, U reduction and removal from pore water is usually seen within the Fe reduction zone (Barnes and Cochran, 1990; Barnes and Cochran, 1991; Scholz et al., 2011). As such, a downward diffusive flux of U across the water-sediment interface is expected in reducing sedimentary environment.” A reference to Scholtz et al. (GCA, 2011) was included in the original text which showed clear evidence that a tiny increase in bottom water oxygen concentrations would be sufficient to release U.

195 Line 503: In order to easily compare with GP16, please give the values you estimated here.

Response: Agreed and fixed

200 Line 505: same comment: please say how much were upwelling fluxes accounting for in your study.

Response: We now specified how much upwelling fluxes made up the total ²³⁴Th fluxes in our study.

205 Figure 2: Please add in both the caption and legend what the red line corresponds to.

Response: The caption in the original text stated “Red dashed lines indicate the depth of the mixed layer.” For clarity, we only included data symbols in the legend.

210 Reviewer #2
Second round comments on “Effects of ^{238}U variability and physical transport on the water column ^{234}Th downward fluxes in the coastal upwelling system off Peru” by Xie et al.

Anonymous reviewer #2

215 I am very happy to see this version of the manuscript which I read with more fun than their first version. Most of my concerns has been answered in the new version. There are not too many studies trying to discuss the impact of physical transport on the downward ^{234}Th flux in the open ocean. This study is therefore welcome to the community.

220 Before the acceptance of this paper, I only have one question that I am not satisfied. The authors attributed the abnormal uranium activity to the flooding from the coasts, and they also indicated a high activity of particulate ^{234}Th in those flooding waters. Therefore, the dissolved ^{234}Th in those water should be lowered by the sinking of those riverine particles. Once the water was transferred to the region of sampling, it should represent an integrated signal mostly derived from flooding particle export not just the local marine particle export. Then even we have carefully estimated the horizontal and vertical transport of ^{234}Th , the final ^{234}Th flux is still not
225 induced by the local export. I do not know for this case ^{234}Th is still a good tracer or not?

Response: Please refer to our previous response to this comment in our last revision. We had agreed that flooding is not likely the main source of additional U to our study site. The discussion on U input via flooding had been removed in our last revision, so that the reviewer’s comment is not relevant to the current version of the manuscript.
230

1 (Mark-up version: Changes made in the revision were marked with an
2 underline.)

3 **Effects of ^{238}U variability and physical transport on water column
4 ^{234}Th downward fluxes in the coastal upwelling system off Peru**

5
6 Ruifang C. Xie^{1*}, Frédéric A. C. Le Moigne², Insa Rapp¹, Jan Lüdke¹, Beat Gasser³, Marcus
7 Dengler¹, Volker Liebetrau¹, Eric P. Achterberg¹

8
9 ¹GEOMAR Helmholtz Center for Ocean Research Kiel, Wischhofstrasse 1-3, 24148 Kiel,
10 Germany

11 ²Mediterranean Institute of Oceanography (UM 110, MIO), CNRS, IRD, Aix Marseille
12 Université, Marseille, France

13 ³IAEA Environment Laboratories, 4 Quai Antoine 1er, 98000 Monaco
14 Monaco

15

16 * corresponding author: rxie@geomar.de

17 **Abstract**

18 The eastern boundary region of the southeastern Pacific Ocean hosts one of the world's most
19 dynamic and productive upwelling systems with an associated oxygen minimum zone (OMZ).
20 The variability in downward export fluxes in this region, with strongly varying surface
21 productivity, upwelling intensities and water column oxygen content, is however poorly
22 understood. Thorium-234 (^{234}Th) is a powerful tracer to study the dynamics of export fluxes
23 of carbon and other elements, yet intense advection and diffusion in nearshore environments
24 impact the assessment of depth-integrated ^{234}Th fluxes when not properly evaluated. Here we
25 use VmADCP current velocities, satellite wind speed and *in situ* microstructure measurements
26 to determine the magnitude of advective and diffusive fluxes over the entire ^{234}Th flux budget
27 at 25 stations from 11°S to 16°S in the Peruvian OMZ. Contrary to findings along the
28 GEOTRACES P16 eastern section, our results showed that weak surface wind speed during
29 our cruises induced low upwelling rates and minimal upwelled ^{234}Th fluxes, whereas vertical
30 diffusive ^{234}Th fluxes were important only at a few shallow shelf stations. Horizontal
31 advective and diffusive ^{234}Th fluxes were negligible because of small alongshore ^{234}Th
32 gradients. Our data indicated a poor correlation between seawater ^{238}U activity and salinity.
33 Assuming a linear relationship between the two would lead to significant underestimations of
34 the total ^{234}Th flux by up to 40% in our study. Proper evaluation of both physical transport
35 and variability in ^{238}U activity is thus crucial in coastal ^{234}Th flux studies. Finally, we showed
36 large temporal variations on ^{234}Th residence times across the Peruvian upwelling zone, and
37 cautioned future carbon export studies to take these temporal variabilities into consideration
38 while evaluating carbon export efficiency.

39 **Keywords:** eastern tropical South Pacific, ^{234}Th tracer, uranium-salinity correlation, physical
40 processes, residence time

41 1. Introduction

42 Isotopes of thorium (Th) are widely used as tracers for particle cycling in the oceans
43 (Waples et al., 2006). In particular, ^{234}Th has been extensively used to trace particle dynamics
44 and export fluxes in the upper ocean, and to quantify the marine budgets of important macro-
45 and micronutrients such as carbon (C), nitrogen (N), phosphorus (P) and iron (Fe) (e.g. Bhat
46 et al., 1968; Buesseler et al., 1992; Coale and Bruland, 1987; Lee et al., 1998; Le Moigne et
47 al., 2013; Cochran and Masqué, 2003; Van Der Loeff et al., 2006; Black et al., 2019). ^{234}Th
48 has a relatively short half-life ($\tau_{1/2} = 24.1$ days) that allows studies of biological and physical
49 processes occurring on timescales of days to weeks. Unlike its radioactive parent uranium-238
50 (^{238}U , $\tau_{1/2} = 4.47$ Ga) that is soluble in seawater, ^{234}Th is highly particle reactive with a
51 particle-water partition coefficient of 10^3 to 10^8 (Santschi et al., 2006 and references therein)
52 and is thus strongly scavenged by particles (Bhat et al., 1968). Generally, a deficit of ^{234}Th
53 relative to ^{238}U is observed in the surface ocean and reflects net removal of ^{234}Th due to
54 particle sinking, whereas secular equilibrium between ^{234}Th and ^{238}U is observed for
55 intermediate and deep waters. Integrating this surface ^{234}Th deficit with depth yields the
56 sinking flux of ^{234}Th and, if elemental: ^{234}Th ratios are known, the sinking flux of elements
57 such as C, N, P, Si and trace metals (e.g. Bhat et al., 1968; Buesseler et al., 1998; Buesseler et
58 al., 1992; Coale and Bruland, 1987; Weinstein and Moran, 2005; Buesseler et al., 2006;
59 Owens et al., 2015; Black et al., 2019; Puigcorbé et al., 2020).

60 Various ^{234}Th models have been put forward to study adsorption/desorption,
61 aggregation and export, but single box models that assume negligible ^{234}Th fluxes due to
62 physical transport are commonly used to calculate oceanic ^{234}Th -derived particle fluxes (see
63 detailed review by Savoye et al., 2006). This assumption is typically appropriate in open
64 ocean settings where ^{234}Th fluxes due to advection and diffusion are small relative to the
65 downward fluxes of ^{234}Th associated with particle sinking. However, in upwelling regions

66 such as the equatorial Pacific and coastal systems, advective and diffusive ^{234}Th fluxes may
67 become increasingly important (e.g., Bacon et al., 1996; Buesseler et al., 1998; Buesseler et
68 al., 1995; Dunne and Murray, 1999). For example, in the equatorial Pacific, strong upwelling
69 post El-Niño could account for ~50% of the total ^{234}Th fluxes (Bacon et al., 1996; Buesseler
70 et al., 1995). Ignoring the upwelling term could thus lead to an underestimation of ^{234}Th
71 fluxes by a factor of 2. Conversely, horizontal diffusion carrying recently upwelled, ^{234}Th -
72 replete waters has been shown to balance the upwelled ^{234}Th fluxes in the central equatorial
73 Pacific (Dunne and Murray, 1999). To the contrary, advective and diffusive ^{234}Th fluxes were
74 minimal off the Crozet Islands in the Southern Ocean due to limited horizontal ^{234}Th
75 gradients, long residence time of water masses, and low upwelling rates and diffusivities
76 (Morris et al., 2007).

77 The dynamic nature of coastal processes requires that physical terms should be
78 included in ^{234}Th flux calculation whenever possible. Accurate measurements of current
79 velocities and diffusivities are however challenging and thus direct observations of the effects
80 of physical processes on ^{234}Th distributions in coastal regions are scarce. Limited studies have
81 incorporated advection and diffusion in the nearshore zones of the Arabian Sea (Buesseler et
82 al., 1998), Gulf of Maine (Gustafsson et al., 1998; Benitez-Nelson et al., 2000), the South
83 China Sea (Cai et al., 2008) and Peruvian oxygen minimum zone (OMZ) (Black et al., 2018).
84 In the Arabian Sea, coastal upwelling during the southwest monsoon season could account for
85 over 50% of the total ^{234}Th flux (Buesseler et al., 1998). Horizontal advection has been shown
86 to be substantial in the Inner Cosco Bay of the Gulf of Maine (Gustafsson et al., 1998),
87 whereas offshore advection and diffusion are only important in late summer (Benitez-Nelson
88 et al., 2000). Therefore, the importance of physical processes on the ^{234}Th flux estimate is
89 highly dependent on the seasonal and spatial variability of the current velocities, diffusivities
90 and ^{234}Th gradients. In terms of the Peruvian OMZ, Black et al. (2018) showed that coastal

91 upwelling accounts for >50% of total ^{234}Th fluxes at 12°S ; however, how upwelling ^{234}Th
92 fluxes vary seasonally and spatially in this region is unclear.

93 Another uncertainty in ^{234}Th flux calculations in such region stems from variations on
94 dissolved ^{238}U activities. Generally speaking, U behaves conservatively under open ocean
95 oxic conditions and is linearly correlated with salinity (Chen et al., 1986; Ku et al., 1977;
96 Owens et al., 2011). However, numerous studies have shown that such correlation breaks
97 down in various marine environments including the tropical Atlantic (Owens et al., 2011),
98 Mediterranean Sea (Schmidt and Reys, 1991), and Arabian Sea (Rengarajan et al., 2003).
99 Although it is generally accepted that deviations from the linear ^{238}U -S correlation will lead to
100 differences in the final calculated ^{234}Th fluxes, there is currently little knowledge on how
101 significant these differences could be.

102 In this study, we report vertical profiles of ^{234}Th and ^{238}U along four transects
103 perpendicular to the coastline of Peru (i.e. shelf-offshore transects). We evaluate the ^{238}U -S
104 correlation in low-oxygen waters and how deviations from this correlation impact final ^{234}Th
105 flux estimates. We also assess the spatial and temporal importance of advection and diffusion
106 on ^{234}Th flux estimates.

107

108 **2. Sampling and methods**

109 **2.1 Seawater sampling and analysis**

110 Seawater samples were collected at 25 stations along 4 shelf-offshore transects
111 between 11°S and 16°S in the Peruvian OMZ during two cruises M136 and M138 on board
112 the RV Meteor (Figure 1). Cruise M136 took place in austral autumn (April 11 to May 3,
113 2017) along two main transects at 12°S and 14°S (Dengler and Sommer, 2017). Two stations
114 from M136 (stations 458 and 495) were reoccupied within a week (repeat stations 508 and

115 516, respectively) to evaluate the steady-state assumption in the ^{234}Th flux calculation. The
116 surface sample of the repeat station 508 (reoccupied 4.5 days after station 458) was missing so
117 only results from repeat stations 495 and 516 (occupation interval 1.5 days) were compared
118 and discussed in terms of the non-steady state model (section 3.3). ^{234}Th sampling during
119 cruise M138 was carried out in austral winter (June 1 to July 4, 2017) and focused on four
120 shelf-offshore transects at 11°S , 12°S , 14°S and 16°S .

121 At each station, a stainless-steel rosette with Niskin bottles (Ocean Test Equipment[®])
122 was deployed for sampling of total ^{234}Th in unfiltered seawater and dissolved ^{238}U ($0.2\ \mu\text{m}$
123 pore size, Acropak[®] polycarbonate membrane). High vertical resolution sampling was
124 performed in the upper 200 m where most of the biological activity occurs; additional depths
125 were sampled down to 600 m, or 50 m above the seafloor. Deep seawater at 1000 m, 1500 m,
126 and 2000 m was sampled at three stations to determine the absolute β counting efficiency.
127 Salinity, temperature, oxygen concentrations and fluorescence data (Table S1) were derived
128 from the sensors (Seabird Electronics[®] 9plus system) mounted on the CTD frame (Krahmann,
129 2018; Lüdke et al., in review 2020).

130 Sample collection and subsequent chemical processing and analysis for total ^{234}Th
131 followed protocols by Pike et al. (2005) and SCOR Working Group RiO5 cookbook
132 (<https://cmer.who.edu/>). Briefly, a ^{230}Th yield tracer (1 dpm) was added to each sample (4 L)
133 before Th was extracted with MnO_2 precipitates. Precipitates were filtered onto 25 mm quartz
134 microfiber filters (Whatman[®] QMA, $2.2\ \mu\text{m}$ nominal pore size) and dried overnight at 50°C ,
135 after which they were counted at sea on a Risø[®] low-level beta GM multiscaler until
136 uncertainty was below 3%, and again 6 months later at home laboratory for background ^{234}Th
137 activities. After the second beta counting, filters were digested in an 8M HNO_3 /10% H_2O_2
138 solution (Carl Roth[®], trace metal grade). 10 dpm of ^{229}Th was added to each sample at the
139 beginning of digestion to achieve a 1:1 atom ratio between ^{229}Th : ^{230}Th . Digested samples
140 were diluted in a 2.5% HNO_3 /0.01% HF mixture and ^{229}Th / ^{230}Th ratios were measured using

141 an ICP-MS (ThermoFisher® Element XR) to determine the chemistry yield and final ^{234}Th
142 activities. The average yield was calculated to be $97\% \pm 6\%$ ($n = 247$). For a subset of
143 samples (marked in Table S1) whose analysis failed during initial ICP-MS measurement,
144 anion chromatography (Biorad® AG1x8, 100 – 200 mesh, Poly-Prep columns) was performed
145 to remove Mn from the sample matrix before another ICP-MS analysis. This subset of
146 samples also included three samples (marked in Table S1) whose initial ICP-MS measurement
147 was successful, to test whether anion chromatography affects final ICP-MS results. Identical
148 $^{229}\text{Th}/^{230}\text{Th}$ ratios were measured for samples with and without column chromatography (see
149 Table S1 footnotes for details).

150 Each ^{238}U sample was acidified to pH ~ 1.6 at sea and transported home for analysis.
151 Samples of dissolved ^{238}U were diluted 20 times in 1N HNO_3 at home laboratory and spiked
152 with an appropriate amount of ^{236}U spike to achieve $^{236}\text{U}:^{238}\text{U} \sim 1:1$. Ratios of $^{236}\text{U}:^{238}\text{U}$ were
153 analyzed by ICP-MS (ThermoFisher Element XR) and activities of ^{238}U were calculated using
154 isotope dilution. Seawater certified reference materials (CRMs), CASS-6 and NASS-7, and
155 the International Association for the Physical Sciences of the Oceans (IAPSO) standard
156 seawater were analyzed routinely for uranium concentrations.

157

158 2.2 Flux calculation

159 Assuming a one box model, the temporal change of ^{234}Th activities is balanced by
160 production from ^{238}U , radioactive decay of ^{234}Th , removal of ^{234}Th onto sinking particles, and
161 transport into or out of the box by advection and diffusion (Bhat et al., 1968; Savoye et al.,
162 2006; and references therein):

$$163 \quad \frac{\partial A_{Th}}{\partial t} = \lambda(A_U - A_{Th}) - P + V \quad (1)$$

164 where A_U and A_{Th} are respectively the activities of dissolved ^{238}U and total ^{234}Th , λ is
 165 the decay constant of ^{234}Th , P is the net removal flux of ^{234}Th , and V is the sum of advective
 166 and diffusive fluxes. It is recommended that the time interval between station occupations
 167 should be >2 weeks in order to adequately capture the temporal variability of the mean spatial
 168 gradients rather than small local changes (Resplandy et al., 2012). The solution of Eq. (1)
 169 (Savoie et al., 2006) is

$$170 \quad P = \lambda \left[\frac{A_U(1-e^{-\lambda\Delta t}) + A_{Th1}e^{-\lambda\Delta t} - A_{Th2}}{1-e^{-\lambda\Delta t}} \right] \quad (2)$$

171 where Δt is the time interval between repeat occupations of a station; A_{Th1} and A_{Th2}
 172 are respectively total ^{234}Th activities during the first and second occupation. At times when
 173 repeat sampling is not possible within adequate cruise timeframe, steady state conditions are
 174 generally assumed, i.e. $\frac{\partial A_{Th}}{\partial t} = 0$. In this case, Eq. (1) is simplified into:

$$175 \quad P = \int_0^z \lambda(A_U - A_{Th})dz + V \quad (3)$$

176 The vertical flux of ^{234}Th , P ($\text{dpm m}^{-2} \text{d}^{-1}$), is integrated to the depth of interest. Earlier
 177 studies generally used arbitrarily fixed depths (e.g., the base of mixed layer or ML, and 100
 178 m) for ^{234}Th and POC flux estimates (e.g., Bacon et al., 1996; Buesseler et al., 1992). Recent
 179 studies emphasized the need to normalize POC flux to the depth of euphotic zone (EZ), which
 180 separates the particle production layer in the surface from the flux attenuation layer below
 181 (Black et al., 2018; Buesseler and Boyd, 2009; Rosengard et al., 2015). In the open ocean, the
 182 depth of EZ is generally similar to ML depth. The PAR (Photosynthetically Active Radiation)
 183 sensor was not available during both of our cruises, so that it was not possible to identify the
 184 base of the EZ. For the purpose of this study, the slight difference of the exact depth chosen
 185 (ML vs. EZ) was of little relevance to the significance of physical processes and ^{238}U
 186 variability. Due to sampling logistics, however, we did not sample at the base of the ML, but
 187 5-20 m below the ML. This depth corresponded closely to the EZ depth used in Black et al.

188 (2018) in the same study area during austral spring 2013. For the purpose of comparison with
 189 earlier studies which reported ^{234}Th fluxes at 100 m, we also calculated ^{234}Th fluxes at 100 m
 190 in this study.

191

192 2.3 Quantification of the physical fluxes

193 The physical term V in Eq. (2) is expressed as following:

$$194 \quad V = \int_0^z \left(w \frac{\partial Th}{\partial z} - u \frac{\partial Th}{\partial x} - v \frac{\partial Th}{\partial y} \right) dz + \int_0^z \left(K_x \frac{\partial^2 Th}{\partial x^2} + K_y \frac{\partial^2 Th}{\partial y^2} - K_z \frac{\partial^2 Th}{\partial z^2} \right) dz \quad (3)$$

195 where w is the vertical (i.e. upwelling) velocity (m s^{-1}), u and v respectively the zonal
 196 and meridional current velocities (m s^{-1}), and K_x , K_y , and K_z represent eddy diffusivities ($\text{m}^2 \text{s}^{-1}$)
 197 in zonal, meridional and vertical directions, respectively. $\frac{\partial Th}{\partial z}$, $\frac{\partial Th}{\partial x}$ and $\frac{\partial Th}{\partial y}$ are vertical and
 198 horizontal ^{234}Th gradients ($\text{dpm L}^{-1} \text{m}^{-1}$), and $\frac{\partial^2 Th}{\partial x^2}$, $\frac{\partial^2 Th}{\partial y^2}$ and $\frac{\partial^2 Th}{\partial z^2}$ are respectively the second
 199 derivative of ^{234}Th ($\text{dpm L}^{-1} \text{m}^{-2}$) on the zonal, meridional and vertical directions.

200

201 2.3.1 Estimation of upwelling velocities

202 In the Mauritanian and Peruvian coastal upwelling regions, there is strong evidence
 203 that upwelling velocities in the mixed layer derived from satellite scatterometer winds and
 204 Ekman divergence (Gill, 1982) agree well with those from helium isotope disequilibrium
 205 (Steinfeldt et al., 2015). The parameterization by Gill (1982) considers the baroclinic response
 206 of winds blowing parallel to a coastline in a two-layer ocean. Vertical velocity (w) at the
 207 interface yields

$$208 \quad w = \frac{\tau}{\rho f a} e^{-x/a} \quad (4)$$

209 where τ is the wind stress ($\text{kg m}^{-1} \text{s}^{-2}$) parallel to the coast line, ρ the water density
210 (1023 kg m^{-3}), f the Coriolis parameter (s^{-1}) as a function of latitude, a the first baroclinic
211 Rossby radius (km) and X the distance (km) to the coast.

212 Upwelling velocities were calculated at stations within 60 nautical miles (nm) of the
213 coast, where upwelling is the most significant (Steinfeldt et al., 2015). We used $a = 15 \text{ km}$ for
214 all stations based on the results reported by Steinfeldt et al. (2015) for the same study area.
215 The magnitude of monthly wind stress was estimated from the monthly wind velocities
216 (Smith, 1988):

$$217 \quad \tau = \rho_{air} C_D U^2 \quad (5)$$

218 where ρ_{air} is the air density above the sea surface (1.225 kg m^{-3}), C_D the drag
219 coefficient (10^{-3} for wind speed $< 6 \text{ m s}^{-1}$), and U the wind speed.

220 Monthly wind speed (m s^{-1}) fields from MetOp-A/ASCAT scatterometer sensor with
221 a spatial resolution of 0.25° (Bentamy and Croize-Fillon, 2010) were retrieved from the
222 Centre de Recherche et d'Exploitation Satellitaire (CERSAT), at IFREMER, Plouzané
223 (France) (data version numbers L3-MWF-GLO-20170903175636-01.0 and L3-MWF-GLO-
224 20170903194638-01.0). We assumed a linear decrease of w from base of the mixed layer
225 toward both the ocean surface and 240 m depth (bottom depth of our shallowest station).
226 Upwelling rates at any depth between 0 and 240 m at individual stations could thus be
227 determined once w was estimated. Following (Rapp et al., 2019), an error of 50% was
228 assigned to estimated upwelling velocities to account for uncertainties associated with the
229 spatial structure and temporal variability of the wind field, and the satellite wind product near
230 the coast.

231

232 2.3.2 Estimation of upper-ocean velocities

233 During both cruises a phased-array vessel-mounted acoustic Doppler current profiler
234 (VmADCP; 75 kHz Ocean Surveyor, Teledyne RD-Instruments) continuously measured zonal
235 and meridional velocities in the upper 700 m of the water column (Lüdke et al., in review
236 2020). Post-processing of the velocity data included water track calibration and bottom
237 editing. After calibration, remaining uncertainty of hourly averages of horizontal velocities are
238 smaller than 3 cm s^{-1} (e.g. Fischer et al., 2003). For the horizontal advective flux calculation
239 (Eq. 3), velocities collected within a 10 km radian at inshore stations (St. 353, 428, 458, 475,
240 508, 904, and 907) and within a 50 km radian at offshore stations (Lüdke et al., in review
241 2020) were averaged. Data collected at the same positions within 5 days due to station repeats
242 were also included in the velocity average. As representative for the near-surface flow, we
243 extracted the velocity data from the top 30 m for M136 stations and top 50 m for M138 station
244 (defined as the “top layer” thereafter); these depths correspond to 5-20 m below the base of
245 the ML during each cruise.

246

247 2.3.3 Estimation of vertical and horizontal eddy diffusivities

248 While the strength of ocean turbulence determines the magnitude of diapycnal or
249 vertical eddy diffusivities, the intensity of meso- and submesoscale eddies determine the
250 magnitude of lateral eddy diffusivities. During the R/V Meteor cruise M136 and the follow up
251 cruise (M137) in the same region, the strength of upper-ocean turbulence was measured using
252 shear probes mounted to a microstructure profiler. The loosely-tethered profiler was
253 optimized to sink at a rate of 0.55 m s^{-1} and equipped with three shear sensors, a fast-response
254 temperature sensor, an acceleration sensor, two tilt sensors and conductivity, temperature,
255 depth sensors sampling with a lower response time. On transit between each CTD station 3 to
256 9 microstructure profiles were collected. Standard processing procedures were used to
257 determine the dissipation rate of turbulent kinetic energy (ϵ) in the water column (see

258 Schafstall et al., 2010 for detailed description). Subsequently, turbulent vertical diffusivities
259 K_z were determined from $K_z = \Gamma \varepsilon N^{-2}$ (Osborn, 1980), where N is stratification and Γ is the
260 mixing efficiency for which a value of 0.2 was used following Gregg et al. (2018).
261 Stratification (Buoyancy frequency) was calculated using CTD data retrieved from
262 microstructure profilers and following the gsw_Nsquared function from the Gibbs Sea Water
263 library (McDougall et al., 2009; Roquet et al., 2015). A running mean of 10 dbar was applied
264 to avoid including unstable events due to turbulent overturns. The 95% confidence intervals
265 for averaged K_z values were determined from Gaussian error propagation following Schafstall
266 et al. (2010).

267 Altogether, 189 microstructure profiles were collected during M136 (Thomsen and
268 Lüdke, 2018) and 258 profiles during the follow-up cruise M137 (unpublished data; May 6 –
269 29, 2017). An average turbulent vertical diffusivity profile was calculated each from all
270 inshore (<500m water depth) and all offshore (>500m water depth) profiles (Figure S1).
271 Microstructure profiles collected during cruise M138 were not available but there were little
272 variations amongst the cruise average inshore and offshore microstructure profiles from M136
273 and M137 despite drastic change in the intensities of the poleward Peru Chile Undercurrent
274 (Lüdke et al., in review 2020). It thus appears appropriate to apply these average vertical
275 diffusivities also to stations during M138.

276 Horizontal eddy diffusivity could not be determined from data collected during the
277 cruises. Surface eddy diffusivities in the North Atlantic OMZ were estimated to be on the
278 order of a few $1000 \text{ m}^2 \text{ s}^{-1}$ that decrease exponentially with depth (Hahn et al., 2014). Similar
279 magnitude of eddy diffusivities was estimated for the ETSP based on surface drifter data and
280 satellite altimetry (Abernathey and Marshall, 2013; Zhurbas and Oh, 2004). We thus consider
281 an eddy diffusivity of $1000 \text{ m}^2 \text{ s}^{-1}$ as a good approximate in this study for the evaluation of
282 horizontal diffusive ^{234}Th fluxes.

283

284 2.4 Residence time of ^{234}Th

285 The residence time (τ_{Th}) of total ^{234}Th represents a combination of the time required
286 for the partition of dissolved ^{234}Th onto particulate matter and that for particle removal. In a
287 one-box model, the residence time of an element of interest can be estimated by determining
288 the standing stock of this element and the rates of elemental input to the ocean or the rate of
289 elemental removal from seawater to sediments (Bewers and Yeats, 1977; Zimmerman, 1976):

$$290 \quad \tau_{\text{Th}} = \frac{A_{\text{Th}(\text{mean})} \cdot Z}{P} \quad (6)$$

291 For the case of ^{234}Th , $A_{\text{Th}(\text{mean})}$ is the averaged ^{234}Th activities of the surface layer, Z is
292 the depth of top layer, and P the removal flux of ^{234}Th .

293

294 **3. Results**

295 3.1 Profiles of dissolved ^{238}U , total ^{234}Th , oxygen and fluorescence

296 The vertical profiles of ^{238}U and ^{234}Th activities are shown in Figure 2 and tabulated in
297 Table S1. Data from station 508 were reported in Figure 2 and Table S1 but excluded in the
298 Discussion section, because the surface sample at 5 m from this station was missing, which
299 prevents any flux calculation. Also tabulated in Table S1 are temperature, salinity and
300 concentrations of oxygen and fluorescence obtained from the CTD sensors. Uranium
301 concentrations of CRMs and the IAPSO standard seawater are reported in Table S2.

302 Activities of ^{238}U showed small to negligible variations with depth, averaging $2.54 \pm$
303 0.05 dpm L^{-1} (or $3.28 \pm 0.07 \text{ ng/g}$, 1SD, $n = 247$) at all stations. The vertical distributions of
304 ^{238}U did not appear to be affected by water column oxygen concentrations or the extent of
305 surface fluorescence maxima (Figure 2). Average U concentrations of both CASS-6 ($2.77 \pm$

306 0.04 ng g⁻¹, 1SD, n = 5) and NASS-7 (2.86 ± 0.05 ng/g, 1SD, n = 5) measured in this study
307 agreed well with certified values (2.86 ± 0.42 ng g⁻¹ and 2.81 ± 0.16 ng g⁻¹, respectively).
308 Average ²³⁸U concentration measured in our IAPSO standard seawater (OSIL batch P156)
309 (3.24 ± 0.06 ng g⁻¹, 1SD, n = 27) is slightly higher than that reported in Owens et al. (2011)
310 (3.11 ± 0.03 ng g⁻¹, 1SD, n = 10, OSIL P149), and may reflect slight differences in U
311 concentrations between different OSIL batches.

312 Total ²³⁴Th activities varied from 0.63 to 2.89 dpm L⁻¹ (Figure 2). All stations showed
313 large ²³⁴Th deficits in surface waters with ²³⁴Th/²³⁸U ratios as low as 0.25 (Figure 3). The
314 extent of surface ²³⁴Th deficits did not vary as a function of depths of either mixed layer or the
315 upper oxic-anoxic interface, nor the magnitude of surface fluorescence concentrations (Table
316 1, Figure 2). ²³⁴Th at all stations generally reached equilibrium with ²³⁸U at depths between 30
317 m and 250 m (Table 1). The equilibrium depths were slightly shallower toward the shelf at the
318 11°S, 12°S and 16°S transects. At St. 912, deficits of ²³⁴Th extended beyond 600 m depth
319 (Figure 2). The following stations (St. 428, 879, 898, 906, 907, 915, 919) displayed a
320 secondary ²³⁴Th deficit below the equilibrium depth, indicative of ²³⁴Th removal processes. A
321 small ²³⁴Th excess at depth was only observed for St. 559 at 100 m. Ratios of ²³⁴Th/²³⁸U for
322 deep samples at 1000 m, 1500 m, and 2000 m varied between 0.95 and 1.02 (1.00 ± 0.04,
323 1SD, n = 11), suggesting that ²³⁴Th was at equilibrium with ²³⁸U at these depths.

324

325 3.2 Vertical and horizontal ²³⁴Th gradients

326 Discrete vertical ²³⁴Th gradients in each profile (or the curvature of the profile) were
327 estimated by the difference in ²³⁴Th activities and that in sampling depths. As such, vertical
328 ²³⁴Th gradients varied greatly amongst stations, and were larger at shallow depths ranging

329 from 0.003 dpm L⁻¹ m⁻¹ to 0.085 dpm L⁻¹ m⁻¹ (median 0.013 dpm L⁻¹ m⁻¹). Vertical ²³⁴Th
330 gradients were essentially negligible at and below equilibrium depths.

331 While calculation of the vertical ²³⁴Th gradient is straightforward, the same is hardly
332 true for the determination of horizontal ²³⁴Th gradient. Mean ²³⁴Th activities in the top layer
333 (see section 2.3.2 for depth definition) of the water column are highly variable amongst
334 stations (Table 3, Figure 4), and likely reflect variations occurring at small temporal and
335 spatial scales in the Peruvian OMZ. Quantification of the horizontal ²³⁴Th gradient between
336 individual station thus may not be adequate to evaluate large scale advection and eddy
337 diffusion across the study area. Therefore, alongshore ²³⁴Th gradients on a larger spatial scale
338 (1° apart) were instead calculated by grouping stations into 1° by 1° grids and averaging ²³⁴Th
339 activities of each grid for the top layer. Alongshore ²³⁴Th gradients in the top layer at
340 nearshore stations for M138 are fairly consistent, ranging from 1.5 x 10⁻⁶ dpm L⁻¹ m⁻¹ to 1.7 x
341 10⁻⁶ dpm L⁻¹ m⁻¹, with a slightly stronger gradient in the north compared to the south. The net
342 difference in alongshore ²³⁴Th gradient is merely 2 x 10⁻⁷ dpm L⁻¹ m⁻¹. A slightly smaller
343 alongshore ²³⁴Th gradient of 4.8 x 10⁻⁷ dpm L⁻¹ m⁻¹ was observed for M136. The magnitude of
344 the net difference in alongshore ²³⁴Th gradient for M136 cannot be adequately quantified, due
345 to smaller spatial sampling coverage. Judging on the similarity in the spatial distributions of
346 mean ²³⁴Th between cruises M136 and M138 (Figure 4), it is reasonable to assume that net
347 difference in alongshore ²³⁴Th gradient remained similar during both cruises.

348

349 3.3 Steady state vs. non-steady state models

350 The relative importance of ²³⁴Th fluxes due to advection and diffusion were assessed
351 here assuming steady state conditions, which assume negligible temporal ²³⁴Th variability.
352 But how valid is this assumption in the Peruvian upwelling zone? Profiles of temperature and
353 oxygen at repeat stations 458 and 508 showed that a lightly cooler and oxygen-depleted water

354 mass dominated at the upper 50 m at station 508 (Figure 5). However, an assessment of the
355 ^{234}Th fluxes at these two stations were not possible as the surface sample from station 508 was
356 missing. Repeat stations 495 and 516 show substantial temporal variations in ^{234}Th activities
357 at each sampled depth in the top 200 m, while temperature and salinity profiles confirmed that
358 similar water masses were sampled during both occupations (Figure 5). Particularly, the
359 surface ^{234}Th deficit was more intense at St. 495 ($^{234}\text{Th}/^{238}\text{U} = 0.44$) compared to St. 516
360 ($^{234}\text{Th}/^{238}\text{U} = 0.73$). Correspondingly, ^{234}Th fluxes decreased substantially from St. 495 to St.
361 516. At 100 m, the difference in ^{234}Th fluxes between these two stations was $\sim 30\%$ ($3200 \pm$
362 $90 \text{ dpm m}^{-2} \text{ d}^{-1}$ at St. 495 and $2230 \pm 110 \text{ dpm m}^{-2} \text{ d}^{-1}$ at St. 516). At 200 m where ^{234}Th
363 resumed equilibrium with ^{238}U at both stations, ^{234}Th flux difference was $\sim 25\%$ (4510 ± 220
364 $\text{dpm m}^{-2} \text{ d}^{-1}$ at St. 495 and $3455 \pm 200 \text{ dpm m}^{-2} \text{ d}^{-1}$ at St. 516). Taking the non-steady state
365 term in Eq. (1) into consideration (see details in Resplandy et al. (2012) and Savoye et al.
366 (2006) for the derivation of flux formulation and error propagation) increased total ^{234}Th at St.
367 516 by 40% to $3110 \pm 1870 \text{ dpm m}^{-2} \text{ d}^{-1}$ at 100 m (or 45% to $5040 \pm 2290 \text{ dpm m}^{-2} \text{ d}^{-1}$ at 200
368 m), which is indistinguishable within error from fluxes at St. 495. The large errors associated
369 with the non-steady state calculation due to the short duration between station occupations
370 prevent a meaningful application of this model in the current study (also see discussion in
371 Resplandy et al, 2012). As estimation of the physical fluxes is independent of the models
372 chosen between steady and non-steady states, the following results and discussion sections
373 regarding physical effects on the ^{234}Th flux estimates is based on the steady state model only.

374

375 3.4 Export fluxes of ^{234}Th

376 Fluxes of ^{234}Th due to radioactive production and decay (hereafter ‘production flux’),
377 upwelling, and vertical diffusion were reported in Table 1 and Figure 6 for both depths 5-20
378 m below the ML and at 100 m. The production fluxes of ^{234}Th at 5-20 m below the ML

379 ranged from $560 \text{ dpm m}^{-2} \text{ d}^{-1}$ to $1880 \text{ dpm m}^{-2} \text{ d}^{-1}$, whereas at 100 m they were much higher at
380 $850 \text{ dpm m}^{-2} \text{ d}^{-1}$ to $3370 \text{ dpm m}^{-2} \text{ d}^{-1}$. There is no discernable trend regarding the production
381 fluxes between the shelf and offshore stations, similar to those seen along the eastern GP16
382 transect (Black et al. 2017).

383 Alongshore winds were unusually weak off Peru preceding and during our sampling
384 campaign as a result of the 2017 coastal El Niño (Echevin et al., 2018; Lüdke et al., in review
385 2020; Peng et al., 2019), which resulted in nominal upwelling in the water column. At
386 nearshore stations, upwelling rates at the base of the ML varied between $1.3 \times 10^{-7} \text{ m s}^{-1}$ and
387 $9.7 \times 10^{-6} \text{ m s}^{-1}$, whereas upwelling rates at offshore stations were on the order of $10^{-10} \text{ m s}^{-1}$
388 to 10^{-8} m s^{-1} and essentially negligible. As a result, upwelled ^{234}Th fluxes at 5-20 m below the
389 ML were only significant at stations closest to shore; these stations were 428 ($130 \text{ dpm m}^{-2} \text{ d}^{-1}$)
390 1), 883-12 ($80 \text{ dpm m}^{-2} \text{ d}^{-1}$) and 904-16 ($280 \text{ dpm m}^{-2} \text{ d}^{-1}$) whose upwelled ^{234}Th fluxes
391 accounted for 10%, 11% and 25% of the total ^{234}Th fluxes respectively (Figure 6). Upwelled
392 ^{234}Th fluxes at the rest of the stations accounted for less than 2% of the total ^{234}Th fluxes (6%
393 at stations 353 and 907-11) and were insignificant. At 100 m, both vertical ^{234}Th gradients and
394 upwelling rates were significantly smaller compared to shallower depths. As a result,
395 upwelled ^{234}Th fluxes were less than $70 \text{ dpm m}^{-2} \text{ d}^{-1}$, or less than 4% of total ^{234}Th fluxes.

396 Similarly, vertical diffusivities, shown as running mean over 20 m in Figure S1, were
397 an order of magnitude higher at shallow stations ($3.2 \times 10^{-4} \pm 1.7 \times 10^{-4} \text{ m}^2 \text{ s}^{-1}$; 1SD, 27 m to
398 100 m below sea surface) compared to those at deep stations ($1.7 \times 10^{-5} \pm 0.6 \times 10^{-5} \text{ m}^2 \text{ s}^{-1}$;
399 1SD; 34 – 100 m below sea surface). Within the upper 27 m to 33 m layer at offshore deep
400 stations, vertical diffusivities decreased exponentially by an order of magnitude within a few
401 meters; below this depth, vertical diffusivities remained relatively stable (Figure S1). This is
402 not surprising as wind-driven turbulent is most significant at the ocean surface (Buckingham
403 et al., 2019). In this study, the sampling depths immediately below the ML were generally 30

404 m and 60 m. A few high vertical diffusivity values around 30 m at deep stations were unlikely
405 representative for the 30 m – 60 m water column layer. We thus opted to only apply vertical
406 diffusivities below 33 m at deep stations. Relative standard errors (RSE) associated with
407 diffusivity estimates varied from 35% to 55%. Vertical diffusive ^{234}Th fluxes at 5-20 m below
408 the ML, determined using both vertical diffusivity and vertical ^{234}Th gradient, varied greatly
409 amongst stations. At shallow stations 428, 458, and 883-12, vertical diffusive ^{234}Th fluxes
410 made up 37% ($490 \text{ dpm m}^{-2} \text{ d}^{-1}$), 14% ($160 \text{ dpm m}^{-2} \text{ d}^{-1}$), and 21% ($160 \text{ dpm m}^{-2} \text{ d}^{-1}$) of total
411 ^{234}Th fluxes, respectively (Figure 6). At the rest of the stations, vertical diffusive ^{234}Th fluxes
412 appeared to be insignificant, ranging between 1% and 10% in the total ^{234}Th flux budget. At
413 100 m, vertical diffusive ^{234}Th fluxes at station 428, 458, and 883-12 remained high at 390
414 $\text{dpm m}^{-2} \text{ d}^{-1}$, $150 \text{ dpm m}^{-2} \text{ d}^{-1}$, $120 \text{ dpm m}^{-2} \text{ d}^{-1}$, respectively, whereas those at the rest of the
415 stations accounted for < 2% of the total ^{234}Th flux.

416 Horizontal advective and diffusive ^{234}Th fluxes were both very small. Average
417 alongshore current velocities (Lüdke et al., in review 2020) for the top layer varied from 0.06
418 m s^{-1} to 0.34 m s^{-1} . At the peripheral of a freshly-formed anticyclonic eddy (St. 915-1),
419 alongshore current velocities could be as high as 0.53 m s^{-1} . Taking the mean alongshore
420 velocity of 0.2 m s^{-1} and the net difference in alongshore ^{234}Th gradient of $2 \times 10^{-7} \text{ dpm L}^{-1} \text{ m}^{-1}$,
421 the resulting net horizontal advective ^{234}Th flux at the top layer is $\sim 50 \text{ dpm m}^{-2} \text{ d}^{-1}$, a mere
422 3-9% of the total ^{234}Th fluxes.

423 Horizontal diffusive ^{234}Th flux was estimated using an average eddy diffusivity of
424 $1000 \text{ m}^2 \text{ s}^{-1}$ (see Methods section 2.3.3) and the alongshore ^{234}Th gradient. A maximum value
425 of $10 \text{ dpm m}^{-2} \text{ d}^{-1}$ was calculated, which accounted for <1% of total ^{234}Th flux at all stations.
426 Note that the horizontal advective and lateral diffusive fluxes presented here are a rough
427 estimate and should only provide an idea of their order of magnitude. Due to the uncertainty
428 inherent to the estimates, we refrain from adding these values to Table 1.

429

430 **4. Discussion**

431 4.1 Lack of linear ^{238}U – salinity correlation in the Peruvian OMZ

432 The water column profiles of ^{238}U in the Peruvian OMZ (Figure 2) are similar to those
433 seen in the open ocean (see compilations in Owens et al., 2011 and Van Der Loeff et al.
434 (2006), and references therein). It thus appears that water column suboxic/anoxic conditions
435 alone is not sufficient to remove U, in contrast to sedimentary U studies underlying low
436 oxygen waters where soluble U(VI) diffused downward into subsurface sediments and
437 reduced to insoluble U(IV) (Anderson et al., 1989; Böning et al., 2004; Scholz et al., 2011).
438 Our inference is in accord with water column ^{238}U studies in intense OMZs in the eastern
439 tropical North Pacific (Nameroff et al., 2002) and the Arabian Sea (Rengarajan et al., 2003),
440 where ^{238}U concentrations remain constant over the entire upper water column studied.

441 Dissolved ^{238}U and salinity across the entire Peruvian OMZ displayed poor linear
442 correlation regardless of seawater oxygen concentrations (Figure 7a-b). The general consensus
443 is that U behaves conservatively in oxic seawater in the open ocean and early observations
444 have shown that ^{238}U activities can be calculated from salinity based on a simple linear
445 correlation between the two (e.g. Chen et al., 1986; Ku et al., 1977). Compilations in Van Der
446 Loeff et al. (2006) and Owens et al. (2011) further demonstrated that the majority of uranium
447 data points in the global seawater dataset follow a linear correlation with seawater salinity.
448 The ^{238}U -salinity formulations from either Chen et al. (1986) or Owens et al. (2011) are thus
449 generally appropriate for open ocean conditions and have been widely used in ^{234}Th flux
450 studies. However, this linear ^{238}U -salinity correlation breaks down in the Peruvian OMZ.
451 Furthermore, the measured ^{238}U activities in this study correlated poorly with those calculated
452 from salinity using the Owens formulation regardless of water column oxygen concentrations
453 (Table S2, Figure 7c), with the former significantly higher than the projected values and

454 differences up to 10%. Both evidences suggested that non-conservative processes have
455 introduced significant amount of dissolved U into the water column.

456 It is likely that this poor ^{238}U -salinity correlation in the water column is not a unique
457 feature off the coast of Peru. Poor correlations between dissolved ^{238}U and salinity have been
458 previously observed in open ocean settings such as the Arabian Sea (Rengarajan et al., 2003)
459 and the Pacific Ocean (Ku et al., 1977), and shelf-estuary systems such as the Amazon shelf
460 (McKee et al., 1987; Swarzenski et al., 2004). It is possible that the narrow range of salinity
461 within any single ocean basin precludes a meaningful ^{238}U -salinity correlation (Ku et al.,
462 1977; Owens et al., 2011). For the Peruvian shelf system, two possible scenarios may further
463 explain the lack of linear ^{238}U -salinity correlation in the water column. Firstly, authigenic U
464 within the sediments may be remobilized under ENSO-related oxygenation events. In
465 reducing pore water, U reduction and removal from pore water is usually seen within the Fe
466 reduction zone (Barnes and Cochran, 1990; Barnes and Cochran, 1991; Scholz et al., 2011).
467 As such, a downward diffusive flux of U across the water-sediment interface is expected in
468 reducing sedimentary environment. However, pore water and bottom water geochemistry
469 measurements during two previous cruises (M77-1 and M77-2) along an 11°S transect off
470 Peru showed large diffusive fluxes of U out of the Peruvian shelf sediments despite that both
471 Fe reduction and U reduction took place in the top centimeters of sediments (Scholz et al.,
472 2011). It was suggested that a minute increase in bottom water oxygen concentration induced
473 by El Niño events would be sufficient in shifting the U(VI)/U(IV) boundary by a few
474 centimeters and remobilize authigenic U (Scholz et al., 2011). Preceding and during our
475 sampling campaign, a coastal El Niño event, with coastal precipitation as strong as the 1997-
476 98 El Niño event, had developed rapidly and unexpectedly in January, and disappeared by
477 May 2017 during cruise M136 (Echevin et al., 2018; Garreaud, 2018; Peng et al., 2019). This
478 strong coastal El Niño event could induce an oxygenation event large enough to remobilized

479 authigenic U along the Peruvian shelf. Secondly, resuspension of bottom sediments and
480 subsequent desorption of U from ferric-oxyhydroxides could affect the ^{238}U -salinity
481 relationship, similar to that seen on the Amazon shelf at salinity above 10 (McKee et al.,
482 1987) and in laboratory experiments (Barnes and Cochran, 1993). Fe reduction and release
483 from the Peruvian shelf sediments (Noffke et al., 2012; Scholz et al., 2014) could release
484 additional U to overlying waters. The magnitude of such, however, has not been quantified.

485 The consequence of the notable difference between measured ^{238}U in this study and
486 salinity-based ^{238}U to ^{234}Th flux according to Eq. (2) is neither linear nor straightforward,
487 because the vertical gradients of both ^{238}U and ^{234}Th strongly affects the impacts of ^{238}U
488 variations on ^{234}Th fluxes. In this study, ^{234}Th fluxes at 100 m derived from salinity-based
489 ^{238}U lead to significant underestimation of ^{234}Th fluxes by an average of 20% and as high as
490 40% (Table 2). These differences in ^{234}Th fluxes will have direct consequences for ^{234}Th
491 derived elemental fluxes such as C, N, P and trace metals. It is thus important to note that U
492 concentrations in coastal systems are highly sensitive to bottom water oxygen concentrations
493 and redox-related U addition, variability of which is expected to intensify with future climate
494 change (Shepherd et al., 2017). Relatively minor variations in dissolved ^{238}U could account
495 for substantial overestimation/underestimation of the depth-integrated ^{234}Th fluxes. We thus
496 encourage future ^{234}Th flux studies in such environments to include seawater ^{238}U analysis.

497

498 4.2 Dynamic advective and diffusive ^{234}Th fluxes

499 The significance of advection and diffusion in the total ^{234}Th flux budget highly
500 depends on the upwelling rate, current velocity, vertical diffusivity, and ^{234}Th gradient on the
501 horizontal and vertical directions. Our results demonstrated that physical processes off Peru
502 during and post the 2017 coastal El Niño have very limited impact on the downward fluxes of
503 ^{234}Th (Figure 6).

504 Our findings are in reasonable agreement with those from the GEOTRACES GP16
505 eastern section along 12°S from Peru to Tahiti, in which Black et al. (2018) quantified both
506 horizontal and vertical advective ^{234}Th fluxes. Horizontal advective fluxes for the upper 30 m
507 water column estimated during GP16 were $\sim 180 \text{ dpm m}^{-2} \text{ d}^{-1}$ for all nearshore and offshore
508 stations, similar in magnitude to those estimated in our study ($\sim 50 \text{ dpm m}^{-2} \text{ d}^{-1}$). Upwelling
509 fluxes along GP16 eastern section was suggested to account for 50% to 80% of total ^{234}Th
510 fluxes at the base of the euphotic zone (Black et al., 2018), a depth similar to or slightly
511 deeper than ML depths in the current study where upwelling fluxes accounted for less than
512 25% of total ^{234}Th fluxes). Total ^{234}Th fluxes along the GP16 eastern section, ranging from
513 4000 to 5000 $\text{dpm m}^{-2} \text{ d}^{-1}$ at the base of the euphotic zone, were much higher than those in our
514 study (560 to 1900 $\text{dpm m}^{-2} \text{ d}^{-1}$ 5-20 m below the ML). This difference could be related to the
515 period of sampling (austral autumn and winter 2017 in our study vs. austral spring 2013 for
516 the GP16 section). We note that the estimated vertical mixing rates based on ^7Be isotope at
517 the base of the euphotic zone along the GP16 section (Kadko, 2017) were at least an order of
518 magnitude higher than the upwelling rates at the base of the ML at nearby stations in our
519 study. This difference could stem from different methods used to estimate upwelling rates at
520 different timescales, and may also reflect the dynamic upwelling system off Peru in which
521 upwelling rates vary greatly seasonally and interannually. During cruises M136 and M138,
522 upwelling favorable easterly winds off Peru were weak, resulting in negligible coastal
523 upwelling. Coastal upwelling in the same general area was also suggested to be negligible in
524 austral summer 2013 during cruise M92 due to nominal surface wind stress (Thomsen et al.,
525 2016). Results from studies conducted in the same year (October to December 2013, Kadko,
526 2017; December 2012, Steinfeldt et al., 2015; January 2013, Thomsen et al., 2016) indicate
527 that seasonal upwelling rates vary drastically in the Peruvian upwelling zone. The seasonal
528 dynamics of coastal upwelling off Peru are similar to those seen in the Arabian Sea, where
529 large upwelled ^{234}Th fluxes only occurred during mid-late southwest monsoon at stations

530 close to shore (Buesseler et al., 1998). Our findings lend further support to earlier studies that
531 advection and diffusion are seasonally important for ^{234}Th fluxes in regions with high
532 upwelling velocities and diffusivities such as the equatorial Pacific (Bacon et al., 1996;
533 Buesseler et al., 1995; Dunne and Murray, 1999) and coastal sites such as the Arabian Sea
534 (Buesseler et al., 1998) and offshore Peru (Black et al., 2018; this study).

535

536 4.3 Residence time of ^{234}Th in the Peruvian OMZ

537 The residence time calculated using equation (6) was based on a simplified one-
538 dimension (1D) model of Zimmerman (1976). This 1D steady state model is obviously an
539 oversimplification of a multi-dimensional process, it however provides a good first order
540 estimate for understanding the highly dynamic nature of the ^{234}Th residence time. It also
541 provides a reasonable value that can be directly compared to values estimated in earlier ^{234}Th
542 flux studies that did not consider the physical processes. Furthermore, we showed in the
543 Discussion (sections 4.2) that physical processes, namely upwelling and vertical diffusion, are
544 only important at a few shelf stations. We thus consider this simple 1D model robust in
545 estimating the residence time of total ^{234}Th .

546 In this study, residence time of total ^{234}Th in the top layer varied from 20 days at
547 shallow stations to 95 days at deep stations (mean $\tau = 51 \pm 23$ days, 1SD, $n = 24$; Table 3).
548 These values were similar to those estimated within the California Current (Coale and
549 Bruland, 1985) and the residence times of particulate organic carbon (POC) and nitrogen
550 (PON) (Murray et al., 1989), but were much longer than predicted in nearshore shelf waters
551 where residence times of total ^{234}Th were on the order of a few days (Kaufman et al., 1981;
552 Kim et al., 1999; and references therein). The longer residence times estimated in our study
553 could reflect a combination of weak surface ^{234}Th deficits ($^{234}\text{Th} = 0.63$ to 1.82 dpm L^{-1})
554 (Figure 3) and low export fluxes (800 to 2000 dpm $\text{m}^{-2} \text{d}^{-1}$, Figure 7). Nearshore seawater

555 samples during GP16 (Black et al., 2018) featured similar surface ^{234}Th deficits ($^{234}\text{Th} = 0.63$
556 to 1.33 dpm L^{-1}) but much higher downward ^{234}Th fluxes (4000 to $5000 \text{ dpm m}^{-2} \text{ d}^{-1}$) as a
557 result of strong upwelling, implying that residence times of total ^{234}Th in the Peruvian OMZ
558 during GP16 occupation would be 3 – 6 times shorter. Indeed, a quick re-assessment of the
559 GP16 data predicted a shorter residence time of total ^{234}Th of 5 – 23 days within the euphotic
560 zone of the coastal Peruvian OMZ.

561 These temporal variations on the residence times of total ^{234}Th have important
562 implications for the estimation of POC fluxes and quantification of carbon export efficiency.
563 Firstly, seasonal changes in Th residence times reflect variations in particle removal over
564 different integrated timescales. For example, POC produced in surface waters during GP16
565 (austral spring 2013) (Black et al., 2018) would have been exported out of the euphotic zone
566 3-6 times faster than it did during austral autumn 2017 (this study). Secondly, to properly
567 evaluate carbon export efficiency, surface net primary production (NPP) should be averaged
568 over a similar timescale as the residence time of total ^{234}Th during station occupation.
569 Applying a 16-day averaged NPP for export efficiency estimate (Black et al., 2018; Henson et
570 al., 2011) would likely not be appropriate in the current study in which total ^{234}Th fluxes
571 integrated timescales of several weeks. ^{234}Th residence times should thus be properly
572 quantified in coastal studies before deriving export efficiencies over varying NPP integration
573 timescales.

574

575 **5. Conclusions and implications for coastal ^{234}Th flux studies**

576 Advection and diffusion are important in coastal and upwelling regions with respect to
577 ^{234}Th export fluxes (Bacon et al., 1996; Buesseler et al., 1995; Dunne and Murray, 1999;
578 Buesseler et al., 1998). Our findings show that their significance is subject to the seasonal
579 variability of the current and upwelling velocities, diffusivities and ^{234}Th gradients, and

580 should be evaluated on a case-to-case basis. Advective fluxes are perhaps the most
581 straightforward to estimate as current velocities can be obtained routinely from shipboard
582 ADCP measurements and upwelling rates calculated from satellite wind stress (Steinfeldt et
583 al., 2015; Bacon et al., 1996). Horizontal and vertical velocities derived from general ocean
584 circulation models also provide a good first order estimate for advective ^{234}Th fluxes; this
585 approach has been successfully demonstrated in a few studies (Buesseler et al., 1995;
586 Buesseler et al., 1998). In addition, the anthropogenic SF_6 tracer and radium isotopes, widely
587 used to quantify nutrient and Fe fluxes (Charette et al., 2007; Law et al., 2001), as well as ^7Be
588 isotope (Kadko, 2017), could be used independently to constrain horizontal and vertical
589 exchange rates of ^{234}Th (Morris et al., 2007; Charette et al., 2007; Buesseler et al., 2005).
590 When *in situ* microstructure measurements are available (this study), vertical diffusivity can
591 be directly calculated to estimate the vertical diffusive ^{234}Th fluxes. Yet, microstructure
592 analysis is not a routine measurement on oceanographic cruises. Earlier studies in the
593 equatorial Pacific and the Gulf of Maine have shown that general ocean circulation models
594 and a simple assumption on dissipation coefficients could provide a robust estimate on
595 vertical and horizontal diffusivities (Benitez-Nelson et al., 2000; Gustafsson et al., 1998;
596 Charette et al., 2001). Therefore, the calculation of physical fluxes is possible, though
597 challenging, and ^{234}Th fluxes due to physical processes should be carefully considered when
598 conducting research in a coastal and upwelling systems.

599 A striking finding in this study is that the assumption of a linear ^{238}U -salinity
600 correlation could lead to one of the largest errors in ^{234}Th flux estimates. In our study, using
601 the salinity-based ^{238}U activities resulted in significant underestimation of total ^{234}Th fluxes by
602 as much as 40%. Because the translation of ^{238}U activities to ^{234}Th fluxes is not linear, larger
603 differences between measured and salinity-based ^{238}U do not necessarily contribute to greater
604 overestimation or underestimation of ^{234}Th fluxes. For example, moderate difference of 3-6%

605 in ^{238}U throughout the upper 100 m at station 898 lead to 40% difference in final ^{234}Th flux,
606 while a 5-9% difference in ^{238}U at station 906 only resulted in 16% ^{234}Th flux difference
607 (Table 2, S2). We would thus stress the importance of ^{238}U measurements in future ^{234}Th flux
608 studies particularly in coastal and shelf regions.

609 Finally, our study showed that the residence times of total ^{234}Th in the Peruvian
610 nearshore waters varied seasonally. Tropical OMZs are important hotspots for carbon
611 sequestration from the atmosphere and enhanced sedimentary carbon preservation (Arthur et
612 al., 1998; Suess et al., 1987). These OMZs are projected to intensify as a result of future
613 climate change (Keeling and Garcia, 2002; Schmidtko et al., 2017; Stramma et al., 2008).
614 Future studies should take into consideration the large temporal variations of the residence
615 times of total ^{234}Th in order to properly evaluates how carbon biogeochemical cycles and
616 carbon export efficiency in these OMZs will respond to continuing ocean deoxygenation,

617

618 **Data availability**

619 Data are available in supplementary tables and archived at
620 <https://doi.org/10.1594/PANGAEA.921917> (Xie et al., 2020).

621

622 **Author contribution**

623 RCX, FACLM and EAP designed the study. RCX carried out sampling, on-board beta
624 counting of ^{234}Th , and drafted the manuscript. IR conducted ^{234}Th and ^{238}U analyses at home
625 laboratory. JL computed current velocities and vertical diffusivities respectively from
626 VmADCP and microstructure profiler data. All co-authors had a chance to review the
627 manuscript and contributed to discussion and interpretation of the data presented.

628

629 **Competing interests**

630 The authors declare that they have no conflict of interest.

631

632 **Acknowledgements**

633 We thank the crew and science party on board M136 and M138 for their help in sample
634 collection and instrument operation. Thank you to SiaoJean Ko, Dominik Jasinski, André
635 Mutzberg and Mario Esposito for their laboratory assistance. We thank two anonymous
636 reviewers and the associate editor, Marilaure Grégoire, for their constructive comments. The
637 project, cruises, IR, JL and RCX were funded by the German SFB 754 program ('Climate-
638 Biogeochemistry Interactions in the Tropical Ocean'), RCX additionally by a DFG research
639 grant (project number 432469432), and FACLM by a DFG Fellowship of the Excellence
640 Cluster "The Future Ocean" (CP1403). This manuscript benefited from stimulating
641 discussions at the BIARRITZ ('bridging international activity and related research into the
642 twilight zone') workshop held in Southampton, UK in 2019.

References

- 643
644
645 Abernathey, R. P., and Marshall, J.: Global surface eddy diffusivities derived from satellite
646 altimetry, *Journal of Geophysical Research: Oceans*, 118, 901-916,
647 <https://doi.org/10.1002/jgrc.20066>, 2013.
- 648 Anderson, R. F., Fleisher, M. Q., and LeHuray, A. P.: Concentration, oxidation state, and
649 particulate flux of uranium in the Black Sea, *Geochimica et Cosmochimica Acta*, 53, 2215-
650 2224, [https://doi.org/10.1016/0016-7037\(89\)90345-1](https://doi.org/10.1016/0016-7037(89)90345-1), 1989.
- 651 Arthur, M. A., Dean, W. E., and Laarkamp, K.: Organic carbon accumulation and
652 preservation in surface sediments on the Peru margin, *Chemical Geology*, 152, 273-286,
653 [https://doi.org/10.1016/S0009-2541\(98\)00120-X](https://doi.org/10.1016/S0009-2541(98)00120-X), 1998.
- 654 Bacon, M., Cochran, J., Hirschberg, D., Hammar, T., and Fler, A.: Export flux of carbon at
655 the equator during the EqPac time-series cruises estimated from ^{234}Th measurements, *Deep*
656 *Sea Research Part II: Topical Studies in Oceanography*, 43, 1133-1153,
657 [https://doi.org/10.1016/0967-0645\(96\)00016-1](https://doi.org/10.1016/0967-0645(96)00016-1), 1996.
- 658 Barnes, C., and Cochran, J.: Uranium removal in oceanic sediments and the oceanic U
659 balance, *Earth and Planetary Science Letters*, 97, 94-101, [https://doi.org/10.1016/0012-](https://doi.org/10.1016/0012-821X(90)90101-3)
660 [821X\(90\)90101-3](https://doi.org/10.1016/0012-821X(90)90101-3), 1990.
- 661 Barnes, C. E., and Cochran, J. K.: Geochemistry of uranium in Black Sea sediments, *Deep*
662 *Sea Research Part A. Oceanographic Research Papers*, 38, S1237-S1254,
663 [https://doi.org/10.1016/S0198-0149\(10\)80032-9](https://doi.org/10.1016/S0198-0149(10)80032-9), 1991.
- 664 Barnes, C. E., and Cochran, J. K.: Uranium geochemistry in estuarine sediments: Controls on
665 removal and release processes, *Geochimica et Cosmochimica Acta*, 57, 555-569,
666 [https://doi.org/10.1016/0016-7037\(93\)90367-6](https://doi.org/10.1016/0016-7037(93)90367-6), 1993.
- 667 Benitez-Nelson, C. R., Buesseler, K. O., and Crossin, G.: Upper ocean carbon export,
668 horizontal transport, and vertical eddy diffusivity in the southwestern Gulf of Maine,

669 Continental Shelf Research, 20, 707-736, [https://doi.org/10.1016/S0278-4343\(99\)00093-X](https://doi.org/10.1016/S0278-4343(99)00093-X),
670 2000.

671 Bentamy, A., and Croize-Fillon: Gridded surface wind fields from Metop/ASCAT
672 measurements, International Journal of Remote Sensing,
673 DOI:10.1080/01431161.2011.600348, 2010.

674 Bewers, J., and Yeats, P.: Oceanic residence times of trace metals, Nature, 268, 595-598,
675 <https://doi.org/10.1038/268595a0>, 1977.

676 Bhat, S., Krishnaswamy, S., Lal, D., and Moore, W.: $^{234}\text{Th}/^{238}\text{U}$ ratios in the ocean, Earth and
677 Planetary Science Letters, 5, 483-491, [https://doi.org/10.1016/S0012-821X\(68\)80083-4](https://doi.org/10.1016/S0012-821X(68)80083-4), 1968.

678 Black, E. E., Buesseler, K. O., Pike, S. M., and Lam, P. J.: ^{234}Th as a tracer of particulate
679 export and remineralization in the southeastern tropical Pacific, Marine Chemistry, 201, 35-
680 50, <https://doi.org/10.1016/j.marchem.2017.06.009>, 2018.

681 Black, E. E., Lam, P. J., Lee, J. M., and Buesseler, K. O.: Insights From the ^{238}U - ^{234}Th
682 Method Into the Coupling of Biological Export and the Cycling of Cadmium, Cobalt, and
683 Manganese in the Southeast Pacific Ocean, Global Biogeochemical Cycles, 33, 15-36,
684 <https://doi.org/10.1029/2018GB005985>, 2019.

685 Böning, P., Brumsack, H.-J., Böttcher, M. E., Schnetger, B., Kriete, C., Kallmeyer, J., and
686 Borchers, S. L.: Geochemistry of Peruvian near-surface sediments, Geochimica et
687 Cosmochimica Acta, 68, 4429-4451, <https://doi.org/10.1016/j.gca.2004.04.027>, 2004.

688 Buckingham, C. E., Lucas, N. S., Belcher, S. E., Rippeth, T. P., Grant, A. L. M., Le Sommer,
689 J., Ajayi, A. O., and Naveira Garabato, A. C.: The Contribution of Surface and Submesoscale
690 Processes to Turbulence in the Open Ocean Surface Boundary Layer, Journal of Advances in
691 Modeling Earth Systems, 11, 4066-4094, <https://doi.org/10.1029/2019MS001801>, 2019.

692 Buesseler, K., Ball, L., Andrews, J., Benitez-Nelson, C., Belostock, R., Chai, F., and Chao,
693 Y.: Upper ocean export of particulate organic carbon in the Arabian Sea derived from

694 thorium-234, Deep Sea Research Part II: Topical Studies in Oceanography, 45, 2461-2487,
695 [https://doi.org/10.1016/S0967-0645\(98\)80022-2](https://doi.org/10.1016/S0967-0645(98)80022-2), 1998.

696 Buesseler, K. O., Bacon, M. P., Cochran, J. K., and Livingston, H. D.: Carbon and nitrogen
697 export during the JGOFS North Atlantic Bloom Experiment estimated from ^{234}Th : ^{238}U
698 disequilibria, Deep Sea Research Part A. Oceanographic Research Papers, 39, 1115-1137,
699 [https://doi.org/10.1016/0198-0149\(92\)90060-7](https://doi.org/10.1016/0198-0149(92)90060-7), 1992.

700 Buesseler, K. O., Andrews, J. A., Hartman, M. C., Belostock, R., and Chai, F.: Regional
701 estimates of the export flux of particulate organic carbon derived from thorium-234 during the
702 JGOFS EqPac program, Deep Sea Research Part II: Topical Studies in Oceanography, 42,
703 777-804, [https://doi.org/10.1016/0967-0645\(95\)00043-P](https://doi.org/10.1016/0967-0645(95)00043-P), 1995.

704 Buesseler, K. O., Andrews, J., Pike, S. M., Charette, M. A., Goldson, L. E., Brzezinski, M. A.,
705 and Lance, V.: Particle export during the southern ocean iron experiment (SOFeX),
706 Limnology and Oceanography, 50, 311-327, <https://doi.org/10.4319/lo.2005.50.1.0311>, 2005.

707 Buesseler, K. O., Benitez-Nelson, C. R., Moran, S., Burd, A., Charette, M., Cochran, J. K.,
708 Coppola, L., Fisher, N., Fowler, S., and Gardner, W.: An assessment of particulate organic
709 carbon to thorium-234 ratios in the ocean and their impact on the application of ^{234}Th as a
710 POC flux proxy, Marine Chemistry, 100, 213-233,
711 <https://doi.org/10.1016/j.marchem.2005.10.013>, 2006.

712 Buesseler, K. O., and Boyd, P. W.: Shedding light on processes that control particle export
713 and flux attenuation in the twilight zone of the open ocean, Limnology and Oceanography, 54,
714 1210-1232, <https://doi.org/10.4319/lo.2009.54.4.1210>, 2009.

715 Cai, P., Chen, W., Dai, M., Wan, Z., Wang, D., Li, Q., Tang, T., and Lv, D.: A high -
716 resolution study of particle export in the southern South China Sea based on ^{234}Th : ^{238}U
717 disequilibrium, Journal of Geophysical Research: Oceans, 113,
718 <https://doi.org/10.1029/2007JC004268>, 2008.

719 Charette, M. A., Moran, S. B., Pike, S. M., and Smith, J. N.: Investigating the carbon cycle in
720 the Gulf of Maine using the natural tracer thorium 234, *Journal of Geophysical Research:*
721 *Oceans*, 106, 11553-11579, <https://doi.org/10.1029/1999JC000277>, 2001.

722 Charette, M. A., Gonneea, M. E., Morris, P. J., Statham, P., Fones, G., Planquette, H., Salter,
723 I., and Garabato, A. N.: Radium isotopes as tracers of iron sources fueling a Southern Ocean
724 phytoplankton bloom, *Deep Sea Research Part II: Topical Studies in Oceanography*, 54, 1989-
725 1998, <https://doi.org/10.1016/j.dsr2.2007.06.003>, 2007.

726 Chen, J., Edwards, R. L., and Wasserburg, G. J.: ^{238}U , ^{234}U and ^{232}Th in seawater, *Earth and*
727 *Planetary Science Letters*, 80, 241-251, [https://doi.org/10.1016/0012-821X\(86\)90108-1](https://doi.org/10.1016/0012-821X(86)90108-1), 1986.

728 Coale, K. H., and Bruland, K. W.: ^{234}Th : ^{238}U disequilibria within the California Current 1,
729 *Limnology and Oceanography*, 30, 22-33, <https://doi.org/10.4319/lo.1985.30.1.0022>, 1985.

730 Coale, K. H., and Bruland, K. W.: Oceanic stratified euphotic zone as elucidated by ^{234}Th :
731 ^{238}U disequilibria 1, *Limnology and Oceanography*, 32, 189-200,
732 <https://doi.org/10.4319/lo.1987.32.1.0189>, 1987.

733 Cochran, J., and Masqué, P.: Short-lived U/Th series radionuclides in the ocean: tracers for
734 scavenging rates, export fluxes and particle dynamics, *Reviews in Mineralogy and*
735 *geochemistry*, 52, 461-492, <https://doi.org/10.2113/0520461>, 2003.

736 Dengler, M., and Sommer, S.: Coupled benthic and pelagic oxygen, nutrient and trace metal
737 cycling, ventilation and carbon degradation in the oxygen minimum zone of the Peruvian
738 continental margin (SFB 754): Cruise No. M 136 11.04.–03.05. 2017 Callao (Peru)–Callao
739 Solute-Flux Peru I, METEOR-Berichte, DOI: 10.3289/CR_M136, 2017, 2017.

740 Dunne, J. P., and Murray, J. W.: Sensitivity of ^{234}Th export to physical processes in the
741 central equatorial Pacific, *Deep Sea Research Part I: Oceanographic Research Papers*, 46,
742 831-854, [https://doi.org/10.1016/S0967-0637\(98\)00098-3](https://doi.org/10.1016/S0967-0637(98)00098-3), 1999.

743 Echevin, V. M., Colas, F., Espinoza-Morriberon, D., Anculle, T., Vasquez, L., and Gutierrez,
744 D.: Forcings and evolution of the 2017 coastal El Niño off Northern Peru and Ecuador,
745 *Frontiers in Marine Science*, 5, 367, <https://doi.org/10.3389/fmars.2018.00367>, 2018.

746 Fischer, J., Brandt, P., Dengler, M., Müller, M., and Symonds, D.: Surveying the upper ocean
747 with the Ocean Surveyor: a new phased array Doppler current profiler, *Journal of*
748 *Atmospheric and Oceanic Technology*, 20, 742-751, [https://doi.org/10.1175/1520-0426\(2003\)20<742:STUOWT>2.0.CO;2](https://doi.org/10.1175/1520-0426(2003)20<742:STUOWT>2.0.CO;2), 2003.

750 Garreaud, R. D.: A plausible atmospheric trigger for the 2017 coastal El Niño, *International*
751 *Journal of Climatology*, 38, e1296-e1302, <https://doi.org/10.1002/joc.5426>, 2018.

752 Gregg, M., D'Asaro, E., Riley, J., and Kunze, E.: Mixing efficiency in the ocean, *Annual*
753 *review of marine science*, 10, 443-473, DOI: 10.1146/annurev-marine-121916-063643, 2018.

754 Gustafsson, Ö., Buesseler, K. O., Rockwell Geyer, W., Bradley Moran, S., and Gschwend, P.
755 M.: An assessment of the relative importance of horizontal and vertical transport of particle-
756 reactive chemicals in the coastal ocean, *Continental Shelf Research*, 18, 805-829,
757 [https://doi.org/10.1016/S0278-4343\(98\)00015-6](https://doi.org/10.1016/S0278-4343(98)00015-6), 1998.

758 Hahn, J., Brandt, P., Greatbatch, R. J., Krahnemann, G., and Körtzinger, A.: Oxygen variance
759 and meridional oxygen supply in the Tropical North East Atlantic oxygen minimum zone,
760 *Climate dynamics*, 43, 2999-3024, <https://doi.org/10.1007/s00382-014-2065-0>, 2014.

761 Henson, S. A., Sanders, R., Madsen, E., Morris, P. J., Le Moigne, F., and Quartly, G. D.: A
762 reduced estimate of the strength of the ocean's biological carbon pump, *Geophysical Research*
763 *Letters*, 38, DOI: 10.1029/2011gl046735, 2011.

764 Kadko, D.: Upwelling and primary production during the US GEOTRACES East Pacific
765 Zonal Transect, *Global Biogeochemical Cycles*, 31, 218-232,
766 <https://doi.org/10.1002/2016GB005554>, 2017.

767 Kaufman, A., Li, Y.-H., and Turekian, K. K.: The removal rates of ^{234}Th and ^{228}Th from
768 waters of the New York Bight, *Earth and Planetary Science Letters*, 54, 385-392,
769 [https://doi.org/10.1016/0012-821X\(81\)90054-6](https://doi.org/10.1016/0012-821X(81)90054-6), 1981.

770 Keeling, R. F., and Garcia, H. E.: The change in oceanic O_2 inventory associated with recent
771 global warming, *Proceedings of the National Academy of Sciences*, 99, 7848-7853, DOI:
772 10.1073/pnas.122154899, 2002.

773 Kim, G., Hussain, N., and Church, T. M.: How accurate are the ^{234}Th based particulate
774 residence times in the ocean?, *Geophysical research letters*, 26, 619-622,
775 <https://doi.org/10.1029/1999GL900037>, 1999.

776 Ku, T.-L., Knauss, K. G., and Mathieu, G. G.: Uranium in open ocean: concentration and
777 isotopic composition, *Deep Sea Research*, 24, 1005-1017, [https://doi.org/10.1016/0146-
778 6291\(77\)90571-9](https://doi.org/10.1016/0146-6291(77)90571-9), 1977.

779 Law, C., Martin, A., Liddicoat, M., Watson, A., Richards, K., and Woodward, E.: A
780 Lagrangian SF_6 tracer study of an anticyclonic eddy in the North Atlantic: Patch evolution,
781 vertical mixing and nutrient supply to the mixed layer, *Deep Sea Research Part II: Topical
782 Studies in Oceanography*, 48, 705-724, [https://doi.org/10.1016/S0967-0645\(00\)00112-0](https://doi.org/10.1016/S0967-0645(00)00112-0),
783 2001.

784 Le Moigne, F. A. C., Henson, S. A., Sanders, R. J., and Madsen, E.: Global database of
785 surface ocean particulate organic carbon export fluxes diagnosed from the ^{234}Th technique,
786 *Earth Syst. Sci. Data*, 5, 295-304, <https://doi.org/10.5194/essd-5-295-2013>, 2013.

787 Lee, C., Murray, D., Barber, R., Buesseler, K., Dymond, J., Hedges, J., Honjo, S., Manganini,
788 S., Marra, J., and Moser, C.: Particulate organic carbon fluxes: compilation of results from the
789 1995 US JGOFS Arabian Sea process study: By the Arabian Sea carbon flux group, *Deep Sea
790 Research Part II: Topical Studies in Oceanography*, 45, 2489-2501,
791 [https://doi.org/10.1016/S0967-0645\(98\)00079-4](https://doi.org/10.1016/S0967-0645(98)00079-4), 1998.

792 Lüdke, J., Dengler, M., Sommer, S., Clemens, D., Thomsen, S., Krahnmann, G., Dale, A. W.,
793 Achterberg, E. P., and Visbeck, M.: Influence of intraseasonal eastern boundary circulation
794 variability on hydrography and biogeochemistry off Peru, *Ocean Sci. Discuss.*, 2019, 1-31,
795 <https://doi.org/10.5194/os-2019-93>, in review 2020.

796 McDougall, T., Feistel, R., Millero, F., Jackett, D., Wright, D., King, B., Marion, G., Chen,
797 C., Spitzer, P., and Seitz, S.: The International Thermodynamic Equation Of Seawater 2010
798 (TEOS-10): Calculation and Use of Thermodynamic Properties, Global Ship-based Repeat
799 Hydrography Manual, IOCCP Report No, 14, 2009.

800 McKee, B. A., DeMaster, D. J., and Nittrouer, C. A.: Uranium geochemistry on the Amazon
801 shelf: Evidence for uranium release from bottom sediments, *Geochimica et Cosmochimica*
802 *Acta*, 51, 2779-2786, [https://doi.org/10.1016/0016-7037\(87\)90157-8](https://doi.org/10.1016/0016-7037(87)90157-8), 1987.

803 Morris, P. J., Sanders, R., Turnewitsch, R., and Thomalla, S.: ^{234}Th -derived particulate
804 organic carbon export from an island-induced phytoplankton bloom in the Southern Ocean,
805 *Deep Sea Research Part II: Topical Studies in Oceanography*, 54, 2208-2232,
806 <https://doi.org/10.1016/j.dsr2.2007.06.002>, 2007.

807 Murray, J. W., Downs, J. N., Strom, S., Wei, C.-L., and Jannasch, H. W.: Nutrient
808 assimilation, export production and ^{234}Th scavenging in the eastern equatorial Pacific, *Deep*
809 *Sea Research Part A. Oceanographic Research Papers*, 36, 1471-1489,
810 [https://doi.org/10.1016/0198-0149\(89\)90052-6](https://doi.org/10.1016/0198-0149(89)90052-6), 1989.

811 Nameroff, T., Balistrieri, L., and Murray, J.: Suboxic trace metal geochemistry in the eastern
812 tropical North Pacific, *Geochimica et Cosmochimica Acta*, 66, 1139-1158,
813 [https://doi.org/10.1016/S0016-7037\(01\)00843-2](https://doi.org/10.1016/S0016-7037(01)00843-2), 2002.

814 Noffke, A., Hensen, C., Sommer, S., Scholz, F., Bohlen, L., Mosch, T., Graco, M., and
815 Wallmann, K.: Benthic iron and phosphorus fluxes across the Peruvian oxygen minimum
816 zone, *Limnology and Oceanography*, 57, 851-867, <https://doi.org/10.4319/lo.2012.57.3.0851>,
817 2012.

818 Osborn, T.: Estimates of the local rate of vertical diffusion from dissipation measurements,
819 Journal of physical oceanography, 10, 83-89, [https://doi.org/10.1175/1520-0485\(1980\)010<0083:EOTLRO>2.0.CO;2](https://doi.org/10.1175/1520-0485(1980)010<0083:EOTLRO>2.0.CO;2), 1980.

821 Owens, S., Buesseler, K., and Sims, K.: Re-evaluating the ^{238}U -salinity relationship in
822 seawater: Implications for the ^{238}U - ^{234}Th disequilibrium method, Marine Chemistry, 127, 31-
823 39, <https://doi.org/10.1016/j.marchem.2011.07.005>, 2011.

824 Owens, S. A., Pike, S., and Buesseler, K. O.: Thorium-234 as a tracer of particle dynamics
825 and upper ocean export in the Atlantic Ocean, Deep Sea Research Part II: Topical Studies in
826 Oceanography, 116, 42-59, <http://dx.doi.org/10.1016/j.dsr2.2014.11.010>, 2015.

827 Peng, Q., Xie, S.-P., Wang, D., Zheng, X.-T., and Zhang, H.: Coupled ocean-atmosphere
828 dynamics of the 2017 extreme coastal El Niño, Nature Communications, 10, 298, DOI:
829 10.1038/s41467-018-08258-8, 2019.

830 Pike, S., Buesseler, K., Andrews, J., and Savoye, N.: Quantification of ^{234}Th recovery in small
831 volume sea water samples by inductively coupled plasma-mass spectrometry, Journal of
832 Radioanalytical and Nuclear Chemistry, 263, 355-360, <https://doi.org/10.1007/s10967-005-0594-z>, 2005.

834 Puigcorbé, V., Masqué, P., and Le Moigne, F. A. C.: Global database of ratios of particulate
835 organic carbon to thorium-234 in the ocean: improving estimates of the biological carbon
836 pump, Earth Syst. Sci. Data, 12, 1267-1285, DOI: 10.5194/essd-12-1267-2020, 2020.

837 Rapp, I., Schlosser, C., Menzel Barraqueta, J. L., Wenzel, B., Lüdke, J., Scholten, J., Gasser,
838 B., Reichert, P., Gledhill, M., Dengler, M., and Achterberg, E. P.: Controls on redox-sensitive
839 trace metals in the Mauritanian oxygen minimum zone, Biogeosciences, 16, 4157-4182, DOI:
840 10.5194/bg-16-4157-2019, 2019.

841 Rengarajan, R., Sarin, M., and Krishnaswami, S.: Uranium in the Arabian Sea: role of
842 denitrification in controlling its distribution, Oceanologica acta, 26, 687-693,
843 <https://doi.org/10.1016/j.oceact.2003.05.001>, 2003.

844 Resplandy, L., Martin, A. P., Le Moigne, F., Martin, P., Aquilina, A., Mémery, L., Lévy, M.,
845 and Sanders, R.: How does dynamical spatial variability impact ^{234}Th -derived estimates of
846 organic export?, *Deep Sea Research Part I: Oceanographic Research Papers*, 68, 24-45,
847 <https://doi.org/10.1016/j.dsr.2012.05.015>, 2012.

848 Roquet, F., Madec, G., McDougall, T. J., and Barker, P. M.: Accurate polynomial expressions
849 for the density and specific volume of seawater using the TEOS-10 standard, *Ocean*
850 *Modelling*, 90, 29-43, <https://doi.org/10.1016/j.ocemod.2015.04.002>, 2015.

851 Rosengard, S. Z., Lam, P. J., Balch, W. M., Auro, M. E., Pike, S., Drapeau, D., and Bowler,
852 B.: Carbon export and transfer to depth across the Southern Ocean Great Calcite Belt,
853 DOI:10.5194/bg-12-3953-2015, 2015.

854 Santschi, P., Murray, J. W., Baskaran, M., Benitez-Nelson, C. R., Guo, L., Hung, C.-C.,
855 Lamborg, C., Moran, S., Passow, U., and Roy-Barman, M.: Thorium speciation in seawater,
856 *Marine Chemistry*, 100, 250-268, <https://doi.org/10.1016/j.marchem.2005.10.024>, 2006.

857 Savoye, N., Benitez-Nelson, C., Burd, A. B., Cochran, J. K., Charette, M., Buesseler, K. O.,
858 Jackson, G. A., Roy-Barman, M., Schmidt, S., and Elskens, M.: ^{234}Th sorption and export
859 models in the water column: a review, *Marine Chemistry*, 100, 234-249,
860 <https://doi.org/10.1016/j.marchem.2005.10.014>, 2006.

861 Schafstall, J., Dengler, M., Brandt, P., and Bange, H.: Tidal - induced mixing and diapycnal
862 nutrient fluxes in the Mauritanian upwelling region, *Journal of Geophysical Research:*
863 *Oceans*, 115, <https://doi.org/10.1029/2009jc005940>, 2010, 2010.

864 Schmidt, S., and Reyss, J.: Uranium concentrations of Mediterranean seawater with high
865 salinities, *Comptes Rendus de l'Academie des Sciences. Serie 2*, 312, 479-484, 1991.

866 Schmidtko, S., Stramma, L., and Visbeck, M.: Decline in global oceanic oxygen content
867 during the past five decades, *Nature*, 542, 335, DOI: 10.1038/nature21399, 2017.

868 Scholz, F., Hensen, C., Noffke, A., Rohde, A., Liebetrau, V., and Wallmann, K.: Early
869 diagenesis of redox-sensitive trace metals in the Peru upwelling area—response to ENSO-

870 related oxygen fluctuations in the water column, *Geochimica et Cosmochimica Acta*, 75,
871 7257-7276, DOI: 10.1016/j.gca.2011.08.007, 2011.

872 Scholz, F., McManus, J., Mix, A. C., Hensen, C., and Schneider, R. R.: The impact of ocean
873 deoxygenation on iron release from continental margin sediments, *Nature Geosci*, 7, 433-437,
874 <https://doi.org/10.1038/ngeo2162>, 2014.

875 Shepherd, J. G., Brewer, P. G., Oschlies, A., and Watson, A. J.: Ocean ventilation and
876 deoxygenation in a warming world: introduction and overview, *Philosophical Transactions of*
877 *the Royal Society A: Mathematical, Physical and Engineering Sciences*, 375, 20170240,
878 DOI:10.1098/rsta.2017.0240, 2017.

879 Smith, S. D.: Coefficients for sea surface wind stress, heat flux, and wind profiles as a
880 function of wind speed and temperature, *Journal of Geophysical Research: Oceans*, 93,
881 15467-15472, <https://doi.org/10.1029/JC093iC12p15467>, 1988.

882 Steinfeldt, R., Sültenfuß, J., Dengler, M., Fischer, T., and Rhein, M.: Coastal upwelling off
883 Peru and Mauritania inferred from helium isotope disequilibrium, *Biogeosciences*, 12, 7519-
884 7533, <https://doi.org/10.5194/bg-12-7519-2015>, 2015.

885 Stramma, L., Johnson, G. C., Sprintall, J., and Mohrholz, V.: Expanding oxygen-minimum
886 zones in the tropical oceans, *science*, 320, 655-658, DOI: 10.1126/science.1153847, 2008.

887 Suess, E., Kulm, L., and Killingley, J.: Coastal upwelling and a history of organic-rich
888 mudstone deposition off Peru, *Geological Society, London, Special Publications*, 26, 181-197,
889 <https://doi.org/10.1144/GSL.SP.1987.026.01.11>, 1987.

890 Swarzenski, P., Campbell, P., Porcelli, D., and McKee, B.: The estuarine chemistry and
891 isotope systematics of $^{234,238}\text{U}$ in the Amazon and Fly Rivers, *Continental Shelf Research*, 24,
892 2357-2372, <https://doi.org/10.1016/j.csr.2004.07.025>, 2004.

893 Thomsen, S., Kanzow, T., Krahnemann, G., Greatbatch, R. J., Dengler, M., and Lavik, G.: The
894 formation of a subsurface anticyclonic eddy in the Peru - Chile Undercurrent and its impact

895 on the near - coastal salinity, oxygen, and nutrient distributions, Journal of Geophysical
896 Research: Oceans, 121, 476-501, <https://doi.org/10.1002/2015JC010878>, 2016.

897 Van Der Loeff, M. R., Sarin, M. M., Baskaran, M., Benitez-Nelson, C., Buesseler, K. O.,
898 Charette, M., Dai, M., Gustafsson, Ö., Masque, P., and Morris, P. J.: A review of present
899 techniques and methodological advances in analyzing ^{234}Th in aquatic systems, Marine
900 Chemistry, 100, 190-212, <https://doi.org/10.1016/j.marchem.2005.10.012>, 2006.

901 Waples, J. T., Benitez-Nelson, C., Savoye, N., van der Loeff, M. R., Baskaran, M., and
902 Gustafsson, Ö.: An introduction to the application and future use of ^{234}Th in aquatic systems,
903 Marine Chemistry, 100, 166-189, <https://doi.org/10.1016/j.marchem.2005.10.011>, 2006.

904 Weinstein, S. E., and Moran, S. B.: Vertical flux of particulate Al, Fe, Pb, and Ba from the
905 upper ocean estimated from $^{234}\text{Th}/^{238}\text{U}$ disequilibria, Deep Sea Research Part I:
906 Oceanographic Research Papers, 52, 1477-1488, <https://doi.org/10.1016/j.dsr.2005.03.008>,
907 2005.

908 Xie, R. C., Le Moigne, F. A. C., Rapp, I., Lüdke, J., Gasser, B., Degler, M., Liebetrau, V.,
909 and Achterberg, E. P.: Activities of total ^{234}Th and dissolved ^{238}U during cruises M136 and
910 M138 from the Peruvian Oxygen Minimum Zone., PANGAEA,
911 <https://doi.org/10.1594/PANGAEA.921917>, 2020.

912 Zhurbas, V., and Oh, I. S.: Drifter - derived maps of lateral diffusivity in the Pacific and
913 Atlantic oceans in relation to surface circulation patterns, Journal of Geophysical Research:
914 Oceans, 109, <https://doi.org/10.1029/2003JC002241>, 2004.

915 Zimmerman, J. T. F.: Mixing and flushing of tidal embayments in the western Dutch Wadden
916 Sea part I: Distribution of salinity and calculation of mixing time scales, Netherlands Journal
917 of Sea Research, 10, 149-191, [https://doi.org/10.1016/0077-7579\(76\)90013-2](https://doi.org/10.1016/0077-7579(76)90013-2), 1976.

918

919

920 Figure captions

921 Figure 1. Maps showing (a) locations of each station from M136 (white squares) and M138
922 (grey circles) and (B) monthly-averaged current field in the top 15 m from April 16 to May
923 15, 2017 derived from altimetry measurements (<http://marine.copernicus.eu/>; product ID:
924 MULTIOBS_GLO-PHY_REP_015_004). Color boxes in (a) schematically divide the four
925 shelf-offshore transects. Map (a) was created with Ocean Data View (Schlitzer, 2014). The
926 white box in (b) highlights our study area.

927

928 Figure 2. Profiles of ^{238}U (black) and ^{234}Th (orange squares – M136; orange circles – M138)
929 along with concentrations of oxygen (grey) and fluorescence (green). Profiles are organized
930 by cruises, transects, and distance to shore from left to right and top to bottom, indicated by
931 east (E) to west (W) arrows. Error bars for both ^{238}U and ^{234}Th are indicated. Red dashed lines
932 indicate the depth of the mixed layer. The start of the oxygen deficient zone is where oxygen
933 diminishes. Bottom depths are indicated for stations whose bottom depths are shallower than
934 600 m.

935

936 Figure 3. Shelf-offshore distributions of $^{234}\text{Th}/^{238}\text{U}$ along the four studied transects, as shown
937 in Figure 1, for M136 (left) and M138 (right). White dots denote station location.

938

939 Figure 4. Distributions of averaged ^{234}Th activities during M136 (a, top 30 m) and M138 (b,
940 top 50 m).

941

942 Figure 5. Profiles of temperature (solid lines) and salinity (dashed lines) for (a) repeated
943 stations 458 (purple) and 508 (yellow), and (d) 495 (blue) and 516 (orange); (b) and (c)
944 respectively profiles for stations 458 and 508 of ^{238}U (black), ^{234}Th (color squares), and
945 concentrations of oxygen (grey) and fluorescence (green). (e) and (f) respectively profiles for
946 stations 495 and 516 of ^{238}U (black), ^{234}Th (color squares), and concentrations of oxygen
947 (grey) and fluorescence (green).

948

949 Figure 6. Bar charts of ^{234}Th fluxes due to production and decay (blue), upwelling (orange),
950 and vertical diffusion (grey) for the depths at 5 – 20 m below the ML (top) and 100 m below
951 sea surface (bottom). Color boxes corresponds to individual transects in Figure 1. Within each
952 transect stations from west (offshore) to east (nearshore) are listed from left to right. Error
953 bars (1SE) are indicated.

954

955 Figure 7. Cross plots of measured ^{238}U activities vs. salinity for M136 (a) and M138 (b),
956 showing poor linear relationship between ^{238}U and salinity. (c) shows a direct comparison
957 between measured and salinity-based ^{238}U to further highlight the large difference between the
958 two. The solid blue line indicates the 1:1 ratio between measured and projected ^{238}U . Blue
959 dashed lines indicate the \pm errors reported in Owens et al. (2011). Error bars for measured
960 ^{238}U activities are smaller than symbols.

Table 1. ²³⁴Th fluxes due to production and decay, upwelling and vertical diffusion below the mixed layer and at 100 m. Horizontal advective fluxes were not quantified at 100 m. Refer to text for details.

Cruise	Station	Mixed layer			Maximum fluorescence	Equilibrium depth	²³⁴ Th flux at the base of the ML						²³⁴ Th flux at 100 m						
		Cast depth	oxycline depth	depth			Depth	Production and decay	Upwelling	Diffusion	Final flux	1 SD	Production and decay	Upwelling	Diffusion	Final flux	1 SD		
		m	m	m	µg L ⁻¹	m	m	dpm m ⁻² d ⁻¹											
M136	353	1	25	102	1.20	100	30	907	52	-36	923	69	1422	-14	2	1410	189		
M136	380	1	26	129	0.87	80	30	1145	0	-41	1105	54	1637	0	-1	1637	132		
M136	402	1	24	129	7.51	100	30	808	0	-75	732	64	1234	0	2	1236	111		
M136	428	1	10	76	4.11	30	30	983	-128	493	1348	129	1772	33	-390	1415	256		
M136	445	1	17	64	2.07	100	30	820	-10	16	826	66	1621	53	6	1681	165		
M136	458	1	5	55	1.61	100	30	1012	-18	161	1155	117	2101	-11	145	2235	238		
M136	472	1	11	29	7.41	200	40	1887	15	-29	1872	77	3315	-12	63	3366	233		
M136	495	1	18	50	1.13	200	30	1149	1	-19	1130	50	3195	2	-5	3192	89		
M136	516	1	16	45	3.77	200	30	614	0	1	615	49	2229	2	-4	2227	109		
M136	547	1	22	48	1.28	150	30	791	0	85	877	61	2510	0	-15	2495	118		
M136	559	1	20	79	1.70	85	50	623	3	-67	559	117	854	-4	2	852	120		
M136	567	1	21	50	2.40	150	30	1593	0	-23	1570	52	3011	0	-11	3000	86		
M138	879	3	43	93	2.24	200	60	1249	0	-16	1266	91	1702	0	-5	1697	111		
M138	882	10	39	211	2.68	150	50	1321	-7	16	1331	63	2264	19	-12	2272	82		
M138	883	12	10	220	1.31	250	30	683	-84	-159	758	108	1782	31	-121	1692	179		
M138	888	7	41	127	1.59	150	50	1364	0	-120	1244	62	1813	0	-4	1809	86		
M138	892	14	47	128	1.05	100	60	1395	33	-118	1309	72	1743	-3	1	1741	99		
M138	898	1	38	101	1.42	60	50	1099	0	-19	1080	104	1091	0	0	1091	125		
M138	904	16	12	72	3.63	150	20	812	275	0	1087	76	2643	0	-9	2634	79		
M138	906	18	32	81	1.73	200	40	1796	0	4	1799	41	3100	0	-1	3100	77		
M138	907	11	31	100	1.29	60	60	1594	-88	13	1518	147	1787	67	-2	1853	140		
M138	912	3	37	70	2.75	>600	50	1960	0	-79	1881	43	2975	0	-3	2972	78		
M138	915	1	26	99	3.51	200	40	1628	0	22	1650	38	2752	0	0	2752	93		
M138	919	1	19	79	4.46	150	30	1316	0	49	1365	32	3249	0	-8	3241	85		

Table 2. Comparison of ^{234}Th fluxes at 100 m calculated with measured ^{238}U activities and those with salinity-based ^{238}U .

Cruise	Station	Cast	^{234}Th fluxes at 100 m*		Difference %
			measured $\text{dpm m}^{-2} \text{d}^{-1}$	predicted $\text{dpm m}^{-2} \text{d}^{-1}$	
M136	353	1	1422	1320	8
M136	380	1	1637	1304	26
M136	402	1	1234	865	43
M136	428	1	1772	1443	23
M136	445	1	1621	1365	19
M136	458	1	2101	1859	13
M136	472	1	3315	3073	8
M136	495	1	3195	3058	4
M136	516	1	2229	2140	4
M136	547	1	2510	2313	9
M136	559	1	854	751	14
M136	567	1	3011	2879	5
M138	879	3	1702	1515	12
M138	882	10	2264	1875	21
M138	883	12	1782	1352	32
M138	888	7	1813	1441	26
M138	892	14	1743	1257	39
M138	898	1	1091	770	42
M138	904	16	2643	2280	16
M138	906	18	3100	2673	16
M138	907	11	1787	1308	37
M138	912	3	2975	2572	16
M138	915	1	2752	2380	16
M138	919	1	3249	2862	14

* For comparison purposes, we only report here ^{234}Th fluxes due to radioactive production and decay.

Table 3. Residence time of total ^{234}Th in the top layers of Peruvian OMZ.

Cruise	Station	Cast	Average ^{234}Th in	Residence time
			the <u>top</u> layer* dpm L ⁻¹	
M136	353	1	1.48	46
M136	380	1	1.35	35
M136	402	1	1.64	61
M136	428	1	1.57	35
M136	445	1	1.64	61
M136	458	1	1.45	38
M136	472	1	0.93	20
M136	495	1	1.20	31
M136	516	1	1.74	85
M136	547	1	1.67	63
M136	559	1	1.75	94
M136	567	1	1.41	45
M138	879	3	1.59	75
M138	882	10	1.81	69
M138	883	12	1.87	74
M138	888	7	1.68	67
M138	892	14	1.69	65
M138	898	1	1.66	92
M138	904	16	1.32	24
M138	906	18	1.15	25
M138	907	11	1.04	41
M138	912	3	1.25	33
M138	915	1	1.16	28
M138	919	1	1.17	26

* Here 'the top layer' refers to the top 30 m during M136 and top 50 m during M138.

Figure 1

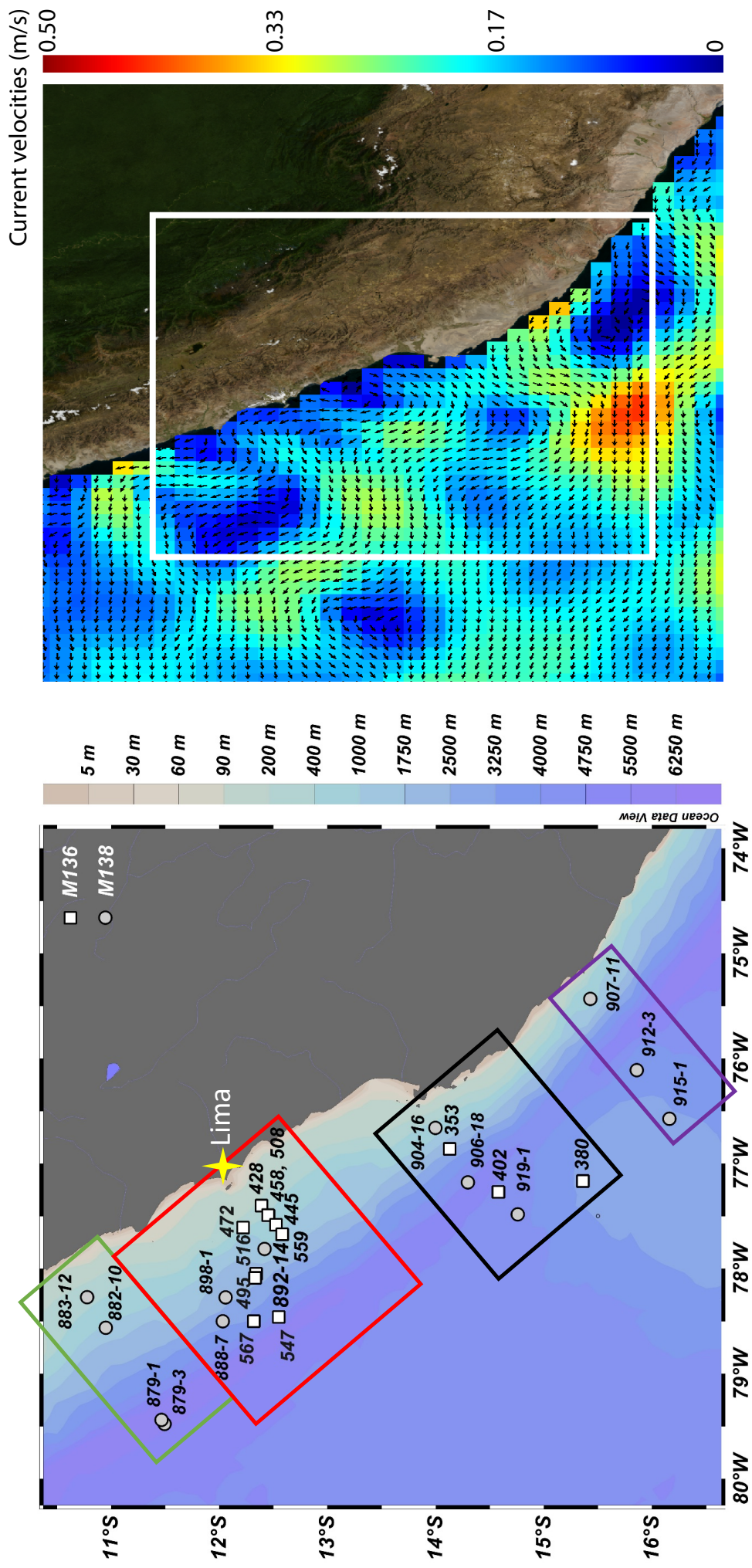
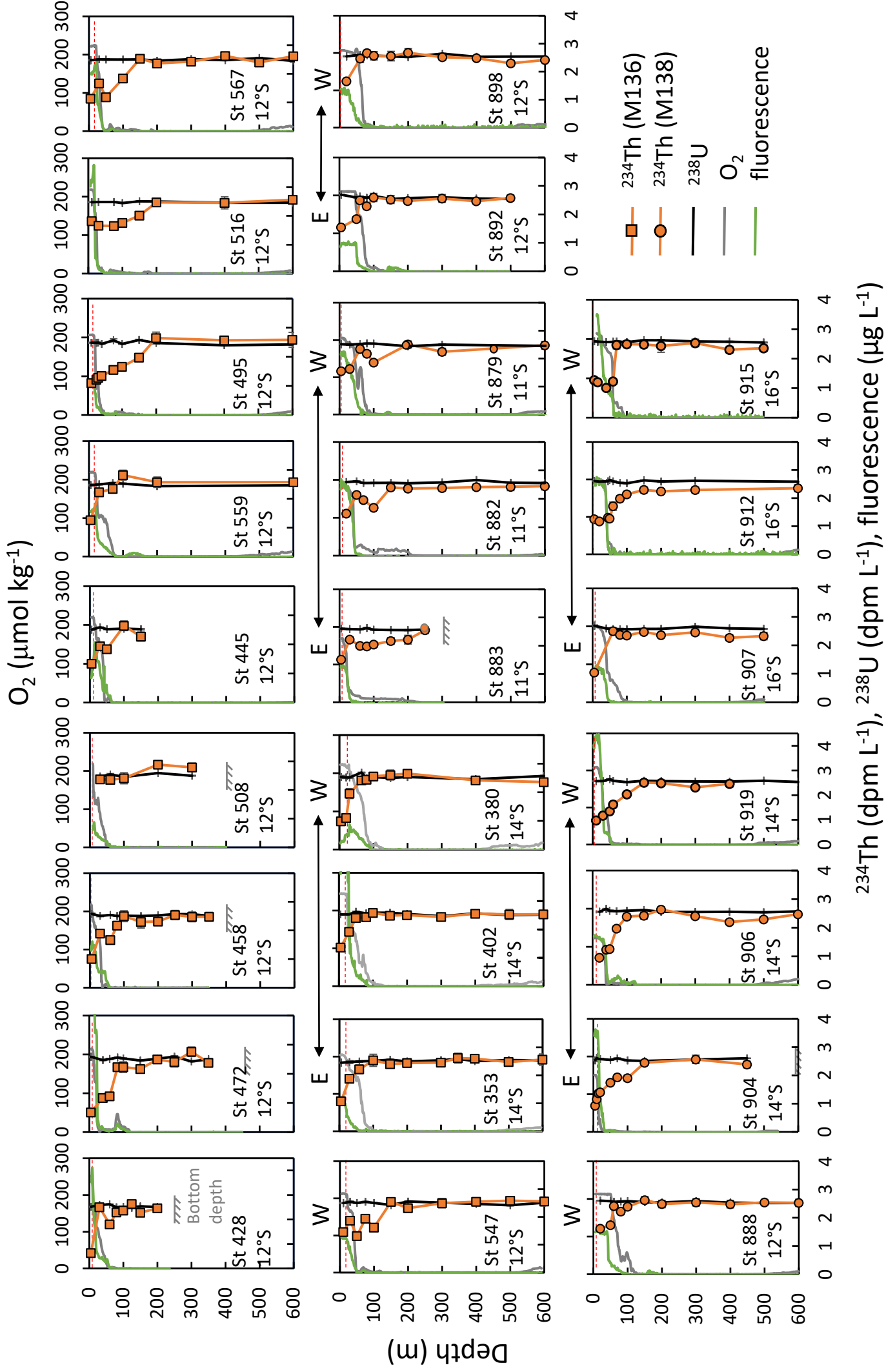


Figure 2

E ← → W



^{234}Th (dpm L^{-1}), ^{238}U (dpm L^{-1}), fluorescence ($\mu\text{g } L^{-1}$)

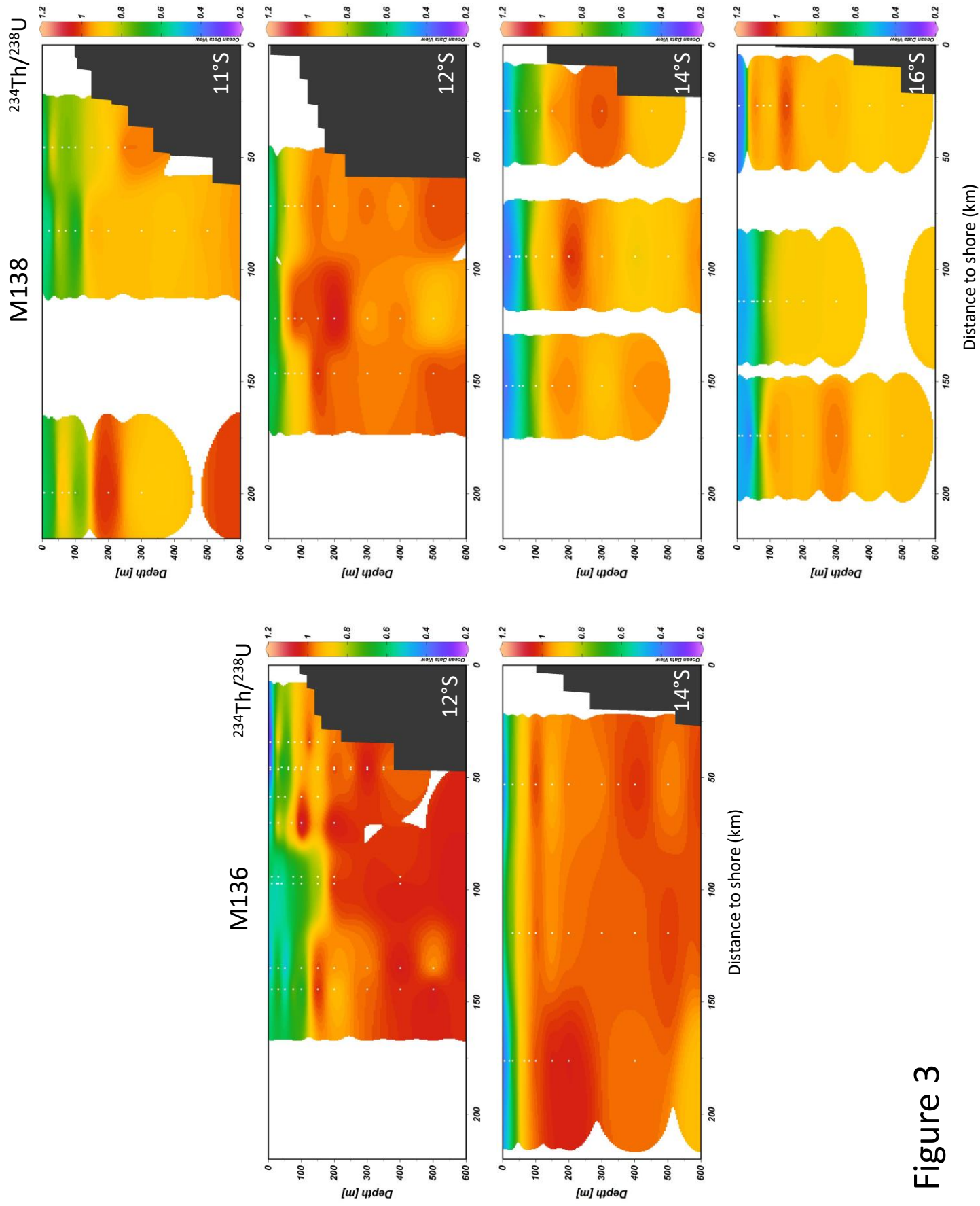


Figure 3

Figure 4

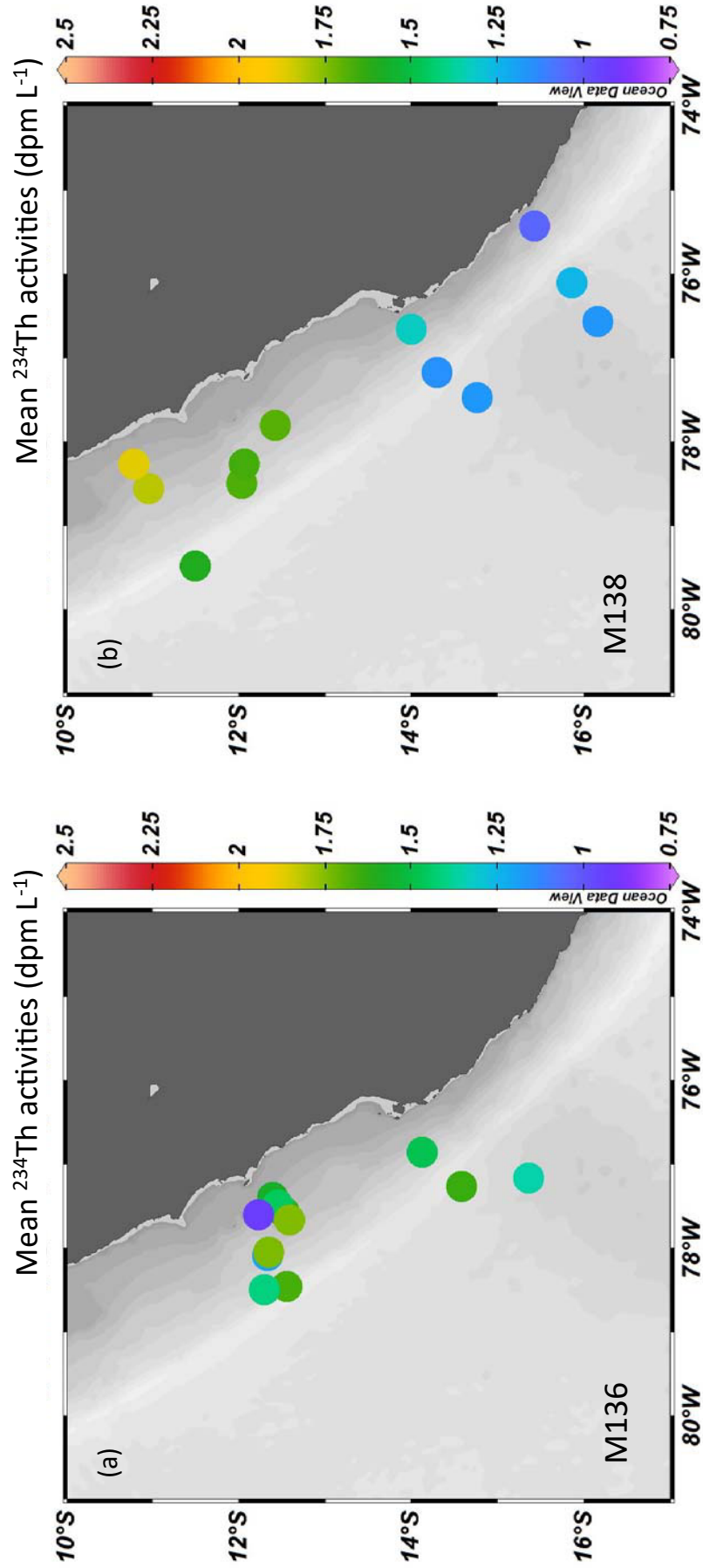


Figure 5

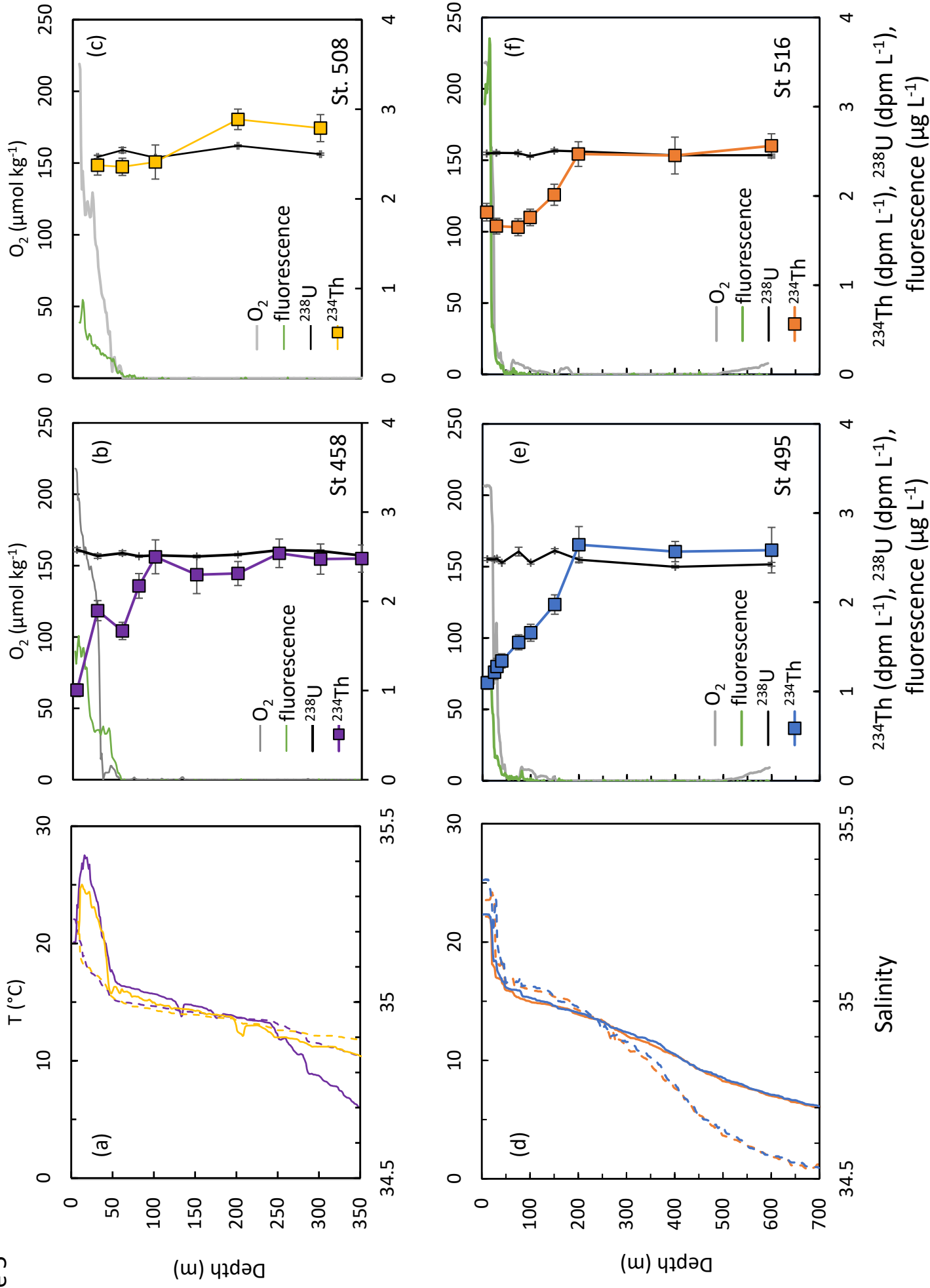


Figure 6

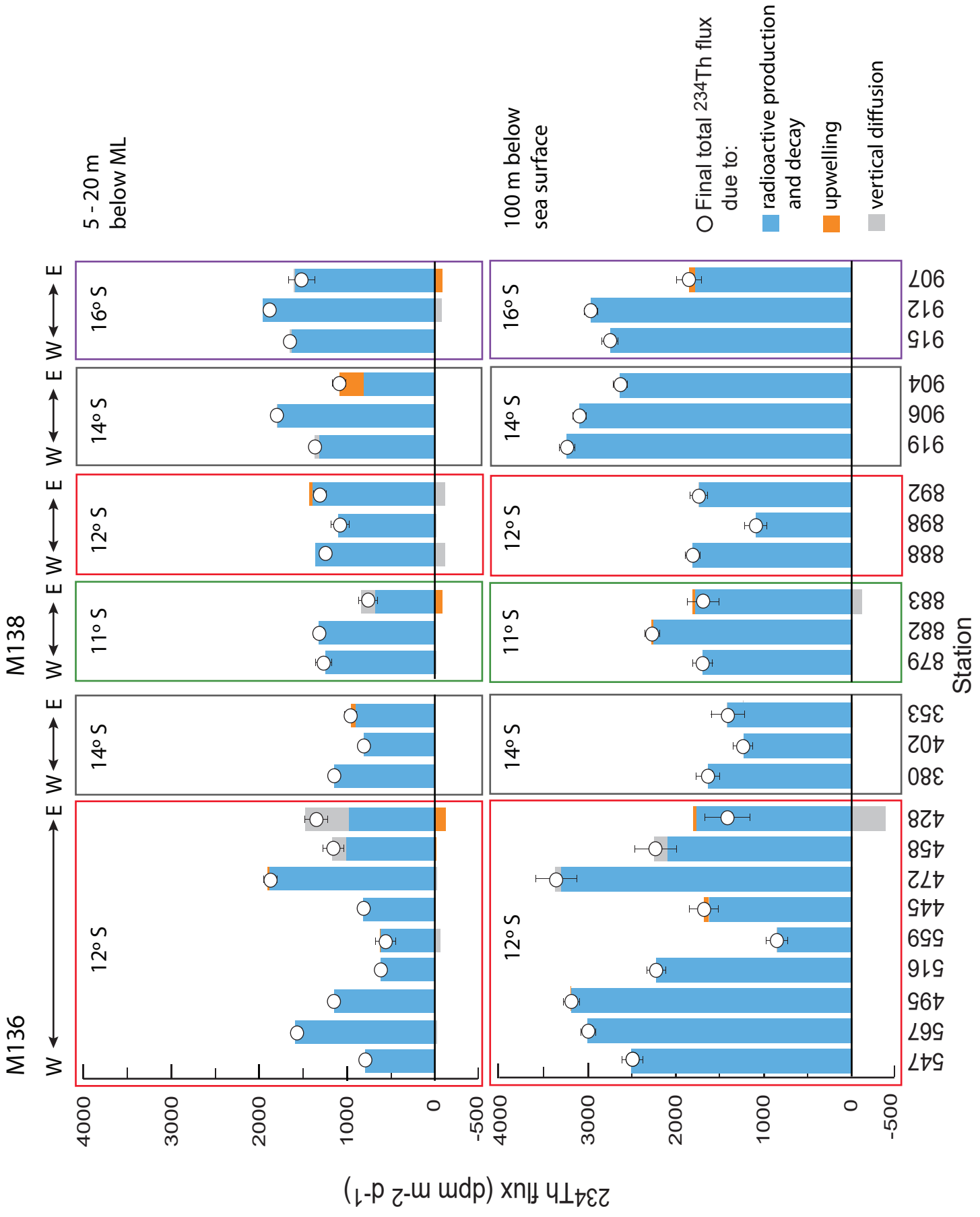


Figure 7

